The genetic architecture of fitness drives population viability during rapid environmental change

Marty Kardos*
Flathead Lake Biological Station
University of Montana
marty.kardos@mso.umt.edu

Gordon Luikart
Flathead Lake Biological Station
University of Montana
gordon.luikart@mso.umt.edu

*Correspondence to marty.kardos@mso.umt.edu
The authors wish to be identified to the reviewers.

Keywords: Adaptation, conservation genomics, extinction, natural selection, climate change, population dynamics, eco-evolutionary dynamics

ABSTRACT

The rapid global loss of biodiversity calls for improved predictions of how population will evolve and respond demographically to ongoing environmental change. The heritability (h^2) of selected traits has long been known to affect evolutionary and demographic responses to environmental change. Here, we show with novel deterministic models and stochastic simulations that the genetic architecture underlying h^2 can dramatically affect population viability during environmental change. Polygenic trait architectures (many loci, each with a small phenotypic effect) conferred higher population viability than when large-effect loci were present under a wide range of scenarios. Population viability depended strongly on the initial frequency of large-effect beneficial alleles, with already-frequent and rare large-effect beneficial alleles conferring lower viability than moderately-low initial allele frequencies. These results suggest that understanding and predicting population responses to human-driven environmental change requires explicitly accounting for the initial h^2 and the underlying genetic architecture of selected traits.

INTRODUCTION

One of the most urgent undertakings for science is to understand how biodiversity will respond to human-driven environmental change (Stockwell *et al.* 2003; Urban *et al.* 2016; Mills *et al.* 2018; Nadeau & Urban 2019). Populations can persist through environmental change either by shifting their geographic distributions to track suitable habitats, or by adapting to changing local conditions (Pease *et al.* 1989). Predicting how populations will evolve and respond demographically to selection imposed by environmental change (e.g., global warming) is a difficult task, but crucial to understanding and mitigating the ongoing extinction crisis (Stockwell *et al.* 2003; Chevin *et al.* 2010; Alberto *et al.* 2013; Urban *et al.* 2016; Funk *et al.* 2018; Shaw 2019).

This need has motivated several theoretical and simulation-based analyses of evolutionary and demographic responses to selection induced by environmental change (Pease *et al.* 1989; Lynch *et al.* 1991; Lynch & Lande 1993; Bürger & Lynch 1995; Gomulkiewicz & Holt 1995; Chevin *et al.* 2010; Gomulkiewicz *et al.* 2010; Nunney 2015; Bay *et al.* 2017). These studies generally combined models of the genetic basis of a selected phenotype, fitness as a function of phenotype, and density-dependent fitness to link adaptation to population dynamics under environmental change. Such models can be used to identify at-risk populations, and to identify the factors that most strongly affect population responses to environmental change and potential resource management strategies to mitigate extinction risk.

Realistic genetic models of variation in selected phenotypes are crucial to inferring evolutionary and demographic responses to selection. The expected phenotypic response per generation has long been known to be proportional to the selected trait's heritability (h^2, the proportion of phenotypic variance due to additive genetic effects). h^2 is therefore a key genetic parameter for modelling evolutionary and demographic responses to environmental change (Lynch & Lande 1993; Gomulkiewicz & Holt 1995; Falconer & Mackay 1996; Chevin *et al.* 2010; Gomulkiewicz *et al.* 2010; Urban *et al.* 2016; Nadeau & Urban 2019). Population genetics theory shows that the genetic architecture of a trait (i.e., the number, distribution of effect sizes, and allele frequencies of the loci underlying h^2) can strongly affect the temporal dynamics of h^2 and set the limits of adaptive phenotype evolution (Figure S1).

Polygenic traits (affected by many loci, each with a small effect) are expected to have higher evolutionary potential than traits with large-effect loci and the same initial h^2. This is because h^2 and the rate of adaptation are expected to decline more rapidly during adaptation for traits with large-effect loci than when a selected trait is polygenic (Barton & Keightley 2002; Walsh & Lynch 2018). This makes the scope for potential adaptive phenotypic evolution generally larger for polygenic traits than for traits with large-effect loci (Figure S1). Populations with polygenic selected phenotypes may therefore be substantially more likely to adapt to new conditions, and to remain viable through environmentally-induced selection than when large-effect loci are responsible for much of the h^2. Knowing the initial h^2 of the selected trait, and using realistic models of the genetic basis of phenotypic variation may therefore be crucial to inferring biological responses to environmental change. However, many previous analyses either didn't explicitly account for h^2, or assumed that h^2 was constant through bouts of selection (Pease *et al.* 1989; Lynch & Lande 1993; Bürger & Lynch 1995; Gomulkiewicz & Holt 1995; Gomulkiewicz *et al.* 2010; Nunney 2015; Bay *et al.* 2017).

Omitting h^2 or the effects of genetic architecture on temporal variation in h^2 may result in unreliable inferences of evolutionary and demographic responses to environmental change. Recent studies show that many fitness-related traits are highly polygenic (Boyle *et al.* 2017). Assuming that h^2 is constant through time despite adaptive evolution – consistent with the infinitesimal model of inheritance in a large population – may be reasonable in such cases. However, many other traits, including some that are likely important for adaptation to climate change (Thompson *et al.* 2019), are governed by loci with very large phenotypic effects (Johnston *et al.* 2013; Barson *et al.* 2015; Kardos *et al.* 2015; Lamichhaney *et al.* 2015; Epstein *et al.* 2016; Lamichhaney *et al.* 2016; Jones *et al.* 2018; Thompson *et al.* 2019). This emerging picture of a large diversity the genetic architecture of fitness traits, and the importance of genetic

architecture to adaptive potential, suggest that including information on both the initial h^2 and the underlying genetic basis of the selected phenotype(s) might substantially improve our understanding and prediction of biological responses to environmental change.

We developed deterministic, theoretical evolutionary-demographic models, and stochastic, individual-based simulations that account for the initial h^2 and the effects of the genetic architecture on temporal change in h^2. We applied these models under a wide range of scenarios to determine when the genetic architecture of a selected phenotype affects the viability of populations subjected to a shifting phenotypic optimum caused by environmental change.

METHODS

A deterministic model of population responses to environmental change

We first develop a deterministic, evolutionary-demographic model that builds upon previous approaches used to investigate evolutionary rescue (Lande 1983; Lynch & Lande 1993; Gomulkiewicz & Holt 1995; Chevin & Lande 2010). We use this model to determine expectations for phenotypic evolution and population growth under a range of simple genetic architectures with purely additive phenotypic effects, unlinked loci, and no epistasis or plasticity.

We model sexually reproducing, non-selfing, diploid populations that have discrete generations and follow a discrete logistic model (May 1974) of density-dependent population growth. Individual fitness is a Gaussian function of a quantitative trait, with the fitness of an individual with phenotype value z being

$$W(z) = W_{\max} e^{-\frac{(z-\theta)^2}{2c^2}}, \qquad (1)$$

where $W_{\max}$ is the fitness (expected lifetime reproductive success) of an individual with optimum phenotype value θ when the population size N is very close to zero, and c^2 defines the width of the fitness function. The population has an initial mean phenotype of $\bar{z}_0$ equal to the initial phenotypic optimum θ_0. The selected phenotype is assumed to be normally distributed with additive genetic (V_G) and random environmental (V_E) variance components summing to the total phenotypic variance V_z ($h^2 = V_G/V_z$). The phenotype's probability density function is

$$P(z) = \frac{1}{\sigma_z\sqrt{2\pi}} e^{-\frac{(z-\bar{z})^2}{2V_z}}, \qquad (2)$$

where $\bar{z}$ is the mean phenotype value, and σ_z the phenotype standard deviation. $\bar{z}$ is calculated as

$$\bar{z} = \theta_0 - \bar{G}_0 + n\sum_{i=1}^{3} f_i' g_i, \qquad (3)$$

where $\bar{G}_0$ is the mean additive genetic phenotype value in the first generation, f_i' is the frequency of the ith of the three possible diploid genotypes, and g_i is the genetic value of the ith of the three possible genotypes, and n the number of diallelic loci affecting the trait. The structure of (3) ensures that the phenotype distribution is centered at θ_0 in the first generation (i.e., $\bar{z}_0 = \theta_0$) and then subsequently allowed to evolve away from θ_0. A sudden environmental change permanently

shifts θ from its initial value θ_0 in the first generation to θ_1, thus imposing directional selection on the phenotype and an environmental challenge to population persistence.

We assume that the allele conferring a larger phenotype (the A1 allele) has the same initial frequency p_0 at each locus. Further, the frequency of the A1 allele(s) is assumed to evolve identically at each of the n loci, such that p in generation $t + 1$ at each locus is

$$p_{t+1} = \frac{p_t \overline{w}_{11} + p_t(1-p_t)\overline{w}_{12}}{\overline{w}_t}, \qquad (4)$$

where $\overline{w}_{11}$ and $\overline{w}_{12}$ represent the mean relative fitness of homozygous A1A1 genotypes, and heterozygous A1A2 genotypes, respectively, and $\overline{w}_t$ is the mean individual fitness in generation t. Mean individual fitness in the population is calculated by integrating over the product of the fitness and phenotype density functions:

$$\overline{w} = \int W(z)P(z)\, dz. \qquad (5)$$

The mean genotype-specific relative fitness (i.e., $\overline{w}_{11}$ or $\overline{w}_{12}$) is calculated as in (5) except with the variance (V_z) and mean ($\bar{z}$) of the phenotype probability density function being conditional on holding the genotype constant at a locus. The V_z conditional on holding the genotype constant at a locus is

$$V_{z,C} = \sum_{i=1}^{n-1} 2p(1-p)a^2 + V_E, \qquad (6)$$

where a is half the phenotypic difference between the two alternative homozygous genotypes. The mean phenotype conditional on holding the genotype constant at a locus is

$$\bar{z}_g = \theta_0 - \bar{G}_0 + g' + (n-1)\sum_{i=1}^{3} f_i' g_i, \qquad (7)$$

where g' is the genetic value of the single-locus genotype being held constant (i.e., $g' = 0$ for genotype A2A2, $g' = a$ for A1A2, and $g' = 2a$ for A1A1). The mean genotype-specific fitness [i.e., $\overline{w}_{11}$ and $\overline{w}_{12}$ in (4)] is calculated as in (5), after first replacing $\bar{z}$ and V_z with $\bar{z}_g$ and $V_{z,C}$ in (2).

We calculate h^2 each generation as

$$h^2 = \frac{\sum_{i=1}^{n} 2p_i(1-p_i)a^2}{V_z}. \qquad (8)$$

Population size (N) in generation $t + 1$ is calculated following the discrete logistic model as

$$N_{t+1} = N_t e^{\left(\ln(\overline{w}_t)\left[1-\frac{N_t}{K}\right]\right)}, \qquad (9)$$

where K is the carrying capacity.

We numerically iterated this model for 80 generations to evaluate the effects of the number of loci underlying h^2 on the evolutionary and demographic responses to a sudden shift in the optimum phenotype due to an environmental change. We first considered simple cases where either 1 or 2 large-effect loci (large-effect architectures), or 100 loci with small effects (polygenic architecture) contributed to V_G. We assumed $h_0^2 = 0.6$, and that each of n loci contributed equally to V_G. We also assume that both $\bar{z}_0$ and θ_0 = 100 (in arbitrary units), $\theta_1 = 110$, the initial population size was $N_0 = 500$, and the carrying capacity was K = 1,000. The initial frequency of positively-selected alleles at each of the n loci was either p_0 = 0.1, 0.25, 0.5, 0.75, or 0.9. We considered a population extinct when N was < 2. Note that this model, and the models below, control for the initial evolvability (mean-scaled additive genetic variance) (Hansen *et al.* 2011) in addition to h_0^2.

While this model is useful for understanding population responses to selection, it makes some assumptions that are unlikely to hold in natural populations (e.g., no selection-induced linkage disequilibrium [LD]). LD among loci affecting a selected phenotype could be substantial, and may affect the pace of adaptation when multiple loci are involved and locus-specific selection is strong (Barton & Turelli 1991). This model (and previous similar models) also assumes that the selected phenotype is normally distributed. However, strong selection and/or large-effect loci might skew the phenotype distribution away from normality (Barton & Turelli 1991). We therefore repeated the above analyses, this time implementing an explicit simulation-based model of genotype and the phenotype distributions for this model (details in Supplementary Materials). The simulated phenotypes were approximately normally distributed (Figure S2).

A stochastic, individual-based simulation model of population responses to environmental change

While deterministic models, such as the ones described above, are useful for understanding expected responses to selection, they do not incorporate the potentially important effects of evolutionary and demographic stochasticity on population responses to a changing environment. We therefore developed a stochastic, individual-based simulation model of evolution and population dynamics under environmentally-induced selection. This model simulates populations forward-in-time with density-dependent fitness and viability selection on a quantitative trait. The initial population size was set to N_0 = 500 individuals, with a carrying capacity of K = 1,000 individuals. Fitness was density-dependent and followed the discrete logistic model of population growth in eq. (9) above. Mates were paired at random, with no self-fertilization allowed. The number of offspring per breeding pair was Poisson distributed with a mean of $\bar{n}_o$ = 4 offspring. Alleles were transferred from parent to offspring following Mendelian probabilities.

Simulating the selected phenotype

The selected phenotype had an initial variance of V_z = 10 and an initial heritability of $h_0^2 = 0.6$. Individual i's phenotype was

$$z_i = \theta_0 - \bar{G}_0 + \sum_{j=1}^{n} c_{ji}\, a_j + \varepsilon_i, \qquad (10)$$

where θ_0 is the specified optimum (and initial mean) phenotype in the first generation, $\bar{G}_0$ is the mean additive genetic value among individuals in the first generation, c_{ji} is individual i's count of

the allele conferring a larger phenotype at the jth locus, and a_j is the phenotypic effect of the positively selected allele at the jth locus, and the environmental effect ε_i is drawn at random from a normal distribution with mean = 0 and variance = V_E. As in eq. (3), the structure of (10) ensures that the selected phenotype distribution is centered around θ_0 in the first generation. We simulated phenotypes as a function of 1, 2, or 100 loci, each with the same initial beneficial allele frequency p_0, and effect size a (consistent with the deterministic models above). We again assumed no dominance or epistatis.

Fitness as a function of phenotype

Each population was subjected to viability selection on the simulated phenotype. The expected (deterministic) fitness (w) for each individual in generation t was calculated as in equation (1) above. The mean deterministic fitness in generation t ($\bar{w}_t$), N_t, and K were applied to equation (9) to find the deterministic expected population size in generation $t + 1$ ($N_{exp,t+1}$, the total expected number of offspring left by generation t). The mean probability of surviving to breeding age among individuals in generation t was then calculated as

$$\bar{s} = \frac{N_{exp,t+1}}{N_t \bar{n}_o}. \qquad (11)$$

The number of individuals in generation t surviving to maturity was calculated as

$$N_{s,t} = \sum_{i=1}^{N_t} r_i \begin{cases} 0 & \text{if } R_i > \bar{s} \\ 1 & \text{if } R_i \leq \bar{s} \end{cases}, \qquad (12)$$

where R_i is a number selected at random from a uniform distribution bounded by 0 and 1 (using the *runif* function in R). $N_{s,t}$ individuals surviving to maturity in generation t are then selected at random from N_t individuals, with sampling weight w, such that individuals with z closer to θ are more likely to survive to maturity. We calculated the extinction rate each generation as the proportion of 500 replicate simulated populations with < 2 individuals remaining. A flow chart summarizing the structure of the individual-based simulation model is shown in Figure S3.

Simulations of alternative life histories and allele frequency distributions

The simulations above assumed that all of the positively-selected alleles conferring a larger phenotype have the same p_0 and equal phenotypic effects. A more realistic situation is likely where a selected phenotype is governed by both large- and small-effect loci across a wide range of initial allele frequencies. We therefore modified our individual-based simulation model to evaluate the effects of genetic architecture on population responses to selection when both large- and small-effect loci with a wide range of initial allele frequencies were present. The selected phenotype had an initial heritability of $h_0^2 = 0.6$. We ran simulations with and without a single large-effect locus. For simulations with a large-effect locus, we attributed 90% of the V_G to the large-effect locus as $2pqa^2 = 0.9V_G$. The remaining 10% of the V_G was split evenly among the other 99 loci. For simulations without a large-effect locus, the V_G was split evenly among all 100 loci. The residual phenotypic variance (V_E) was attributed to random environmental differences among individuals ($V_E = V_z - V_G$; $V_G = h^2 V_z$). The initial frequency of the positively selected, large-effect alleles was drawn at random from a uniform distribution ranging from 0.05 to 0.95. We set these p_0 limits to avoid extremely large phenotypic effects (i.e., extreme values of a) at

large-effect loci. The p_0 values at the small-effect loci were drawn at random from a beta distribution with parameters α and β each set to 0.5 which results in a typical U-shaped allele frequency distribution where most loci had the minor allele at low frequency (Kimura 1984) [p. 147]. These broad allele frequency ranges are motivated by the fact that there is no globally-applicable, *a priori* expectation for the initial frequency distribution of alleles that are beneficial after an environmental change. For example, historically-favored alleles are expected to be found a relatively high frequency on average. Historically disadvantageous alleles, and recently mutated alleles, are expected to be rare. Alleles that were historically neutral, but positively-selected under new conditions, are expected to be found across the entire spectrum of possible frequencies at the onset of selection.

We parameterized these simulations to approximately mimic two divergent life histories typical of large mammals (Mduma *et al.* 1999) (high survival and low fecundity) and corals (Fadlallah 1983) (low survival and high fecundity) to determine if life history strategy affected the results. The maximum fitness ($W_{\max}$ = the expected reproductive success of a perfectly adapted individual at very low population density) was $W_{\max} = 1.5$ for large mammals (mean number of offspring per breeding pair = 4, survival to maturity probability = 0.75), and $W_{\max} = 1.3$ for corals (mean number of offspring per breeding pair = 26; survival to maturity probability = 0.1). Note that $W_{\max}$ is equivalent to the geometric population growth rate (λ) for a perfectly adapted population with N very near zero. We assumed $N_0 = 500$ and $K = 1{,}000$, and $N_0 = 10{,}000$ and $K = 20{,}000$ for simulations of approximate large mammal and coral life histories, respectively. We initially ran 500 coral and large mammal simulation repetitions to evaluate the effects of genetic architecture on the population responses to selection associated with the shifted phenotypic optimum. We ran 1,500 additional simulations with a large-effect locus and 99 small-effect loci affecting the selected phenotype to determine how p_0 of a large-effect locus affected population dynamics.

We varied the parameters in this individual-based simulation model to test whether effects of genetic architecture were similar across a broad range of alternative scenarios. We simulated lower and higher initial heritability of the selected trait (h_0^2=0.4 and 0.8), gene flow from a population where θ was held constant at θ_0, weaker effects at large-effect loci (i.e., the large-effect locus being responsible for 50% and 70% of V_G), a stochastic linear temporal increase in θ (Lynch & Lande 1993) (instead of a sudden shift as above), selection on linked loci (on 10 chromosome pairs), plasticity in the selected phenotype, and we halved the size of the temporal shift in θ. The methodological details of these additional simulation scenarios are described in the Supplementary Materials. R packages implementing the deterministic model and the stochastic simulation models, along with example scripts, are freely available at https://github.com/martykardos/geneticArchPopDynamics.

Statistical analysis

We constructed 95% percentile bootstrap confidence intervals (Efron & Tibshirani 1994) for the proportion of extinct populations in each simulated scenario. First, we randomly resampled η simulated data sets 1,000 times, with replacement, from the η original simulation repetitions. For each of these 1,000 bootstrap samples, we calculated the proportion of the η resampled populations that were extinct ($N < 2$ individuals) in each of the 80 generations. We constructed

the 95% bootstrap confidence intervals for the extinction rate for each of the 80 generations as the 2.5% and 97.5% quantiles from the bootstrap distributions.

RESULTS AND DISCUSSION

Deterministic predictions of evolutionary and demographic responses to environmental change

Results from our deterministic model suggest that the genetic architecture underlying the h^2 of a selected trait strongly affects the evolutionary and demographic responses to a rapid environmentally-induced shift in θ. First, phenotypic evolution and population growth after the onset of selection were highly dependent on the p_0 of large-effect alleles, but relatively insensitive to p_0 when many small-effect loci were involved (Figure 1). For example, populations with a single large-effect locus and $p_0 \geq 0.5$ all went extinct before 30 generations, whereas N eventually approached K in populations with $p_0 < 0.5$. The time to reach $N \approx K$ was approximately 25 generations longer when there was a single large-effect locus and $p_0 = 0.25$ compared to $p_0 = 0.1$ (Figure 1A). With 2 large-effect loci, the expected time to reach $N \approx K$ was nearly identical for $p_0 = 0.1$ and $p_0 = 0.25$. Populations with 2 large-effect loci recovered slowly with $p_0 = 0.5$, and went extinct by 20 generations with $p_0 > 0.5$ (Figure 1B). The rate of adaptation and recovery of population size was much less affected by p_0 when the selected trait was polygenic, with the phenotype approaching θ_1, and N approaching K for all values of p_0 (Figure 1C). Results from analyses of this model with $h_0^2 = 0.4$ and $h_0^2 = 0.8$ were qualitatively equivalent to the results presented here (Figures S4, S5). Repeating these analyses with simulated phenotypes to account for selection-induced LD and any deviation from the assumed normal phenotype distribution did not substantively affect the results (Supplementary Materials, Figure S6).

These results suggest that large-effect loci confer adaptation and demographic recovery from selection that is similar or higher than with a polygenic architecture only when the positively-selected alleles are initially infrequent ($p_0 \approx 0.1 - 0.25$). Additionally, this model suggests that predictions of demographic responses to environmental change will be more reliable when the selected trait(s) is polygenic as doing so does not require precise estimates of the underlying allele frequencies.

Stochastic, simulation-based predictions of evolutionary and demographic responses environmental change

Similar to the deterministic results, our individual-based simulations show that the lowest initial positively-selected, large-effect allele frequency ($p_0 = 0.1$) conferred substantially increased adaptation, demographic recovery, and a lower extinction rate compared to beneficial, large-effect alleles with higher p_0 (Figure 2A, 2B). The polygenic architecture resulted in a lower extinction rate and larger N on average compared to the large-effect genetic architectures for all p_0 values except $p_0 = 0.1$, in which case the large-effect loci resulted in faster adaptive phenotypic evolution and population size recovery from selection (along with lower extinction rates) compared to the polygenic architecture. Repeating these individual-based simulations with $h_0^2 = 0.4$ and $h_0^2 = 0.8$ generated results that agreed qualitatively with those presented here ($h_0^2 = 0.6$) (Figures S7, S8).

Stochastic simulations with alternative life histories and allele frequency distributions
Results from our simulations of populations with variable p_0 are highly similar to the simpler models presented above, with the very large-effect alleles conferring lower adaption, smaller population sizes, and a higher extinction rate on average than when the selected trait was polygenic (Figure 3). For example, the extinction rate at generation 80 was 2.0 times higher with the large-effect locus (64% extinction rate) compared to the polygenic architecture (32% extinction rate) in simulations assuming a large mammal life history. Similarly, the extinction rate was 2.7 times higher among populations with a large-effect locus (72% extinction rate) compared to the polygenic architecture (27% extinction rate) in simulations assuming a coral-like life history.

These simulation results further suggest that the p_0 at large-effect loci strongly affects population dynamics (Figure 4). The average final population sizes were highest for both life histories when p_0 was ~0.1-0.2. The lower population growth with $p_0 < 0.1$ is likely caused by rare, positively-selected alleles frequently being lost to genetic drift as the populations initially declined rapidly due to selection. The weaker evolutionary and demographic response in populations with already-frequent, large-effect beneficial alleles resulted in lower population growth rates and eventual extinction in a large fraction of populations with $p_0 > 0.2$. Strikingly, all of the populations with a coral life history and $p_0 > 0.5$ went extinct by generation 80.

Alternative simulations with lower and higher initial heritability than above, gene flow from a population with a stationary phenotypic optimum, linked loci, weaker effect sizes at large-effect loci, a stochastic linear temporal increase in θ, phenotypic plasticity, or a smaller shift in θ all resulted in polygenic architectures conferring higher population viability on average compared to when large-effect loci were present (Supplementary Materials; Figures S6-S14). However, the increased evolutionary and demographic responses to selection associated with polygenic architecture was smaller when there was immigration from a population with a stationary θ, when the large-effect loci contributed a smaller fraction of the V_G, and when the environmentally-induced shift in the optimum phenotype was smaller (see detailed results in Supplementary Materials). For example, the extinction rate at 80 generations was only 1.53 times higher with a large effect locus than for the polygenic architecture (compared to a 2-fold difference in the simulations of closed populations above) when there were 4 immigrants per generation from a population with a stationary phenotypic optimum (Supplementary Materials, Figure S9; similar results for 8 immigrants/generation are shown in Figure S10). The extinction rate among populations with a large-effect locus explaining only 50% of h^2 was only 1.28 times higher than with a polygenic architecture (Supplementary Materials, Figure S11). For populations with a smaller shift in the phenotypic optimum ($\theta_0 = 100$ and $\theta_1 = 105$ instead of $\theta_0 = 100$ and $\theta_1 = 110$), the extinction rate was 0.13 in the populations with a large effect locus explaining 90% of the V_G, and only 0.002 among populations with a polygenic selected phenotype.

The results from the wide range of analyses above suggest that the genetic architecture underlying the h^2 of a selected trait can strongly affect population viability during environmental change. A robust understanding of the effects of environmental change on population viability will require accounting for the strong effects of trait genetic architecture on evolutionary and population dynamics. When loci with large phenotypic effects are present, the initial frequency

of large-effect beneficial alleles can strongly affect population responses to selection. Polygenic architectures on average conferred higher evolutionary potential, more consistent evolutionary responses to selection, and increased population viability compared to when the selected trait was governed by large-effect loci. Additionally, while predicting how wild populations will respond to ongoing rapid environmental change remains a difficult task, the models and results presented here can inform future theoretical and empirical efforts to understand eco-evolutionary dynamics and the extent of the ongoing extinction crisis.

The influence of genetic architecture on variation in population responses to environmental change will depend on how often fitness traits have loci with large enough effects to reduce h^2 during bouts of adaptation. Recent results from several taxa, including mammals (Johnston *et al.* 2013; Kardos *et al.* 2015; Epstein *et al.* 2016; Jones *et al.* 2018), salmonids (Barson *et al.* 2015; Thompson *et al.* 2019), and birds (Lamichhaney *et al.* 2015; Lamichhaney *et al.* 2016) suggest that very large-effect alleles often influence fitness-related traits in wild populations. Interestingly, seemingly complex fitness-related traits that are often assumed to be polygenic, such as horn size (a sexually-selected, condition-dependent trait) (Johnston *et al.* 2013), migration timing (Thompson *et al.* 2019), and age at maturity (Barson *et al.* 2015), have in some cases turned out to be driven almost entirely by variation at individual loci. It is therefore crucial to quantify the effect sizes and allele frequencies at loci with large effects when they are present in systems where future eco-evolutionary dynamics are of interest.

It can be difficult to predict or measure the frequency of alleles with large beneficial effects under rapid environmental change. For example, large-effect alleles for traits subjected to historical balancing selection are likely to be at intermediate frequencies (Llaurens *et al.* 2017). Recent large-effect mutations are likely to be found at low frequencies. Previously neutral or nearly-neutral alleles that affect fitness in new conditions are likely to be found across the entire spectrum of allele frequencies. Fortunately, increasingly efficient DNA sequencing and improving approaches for conducting genotype-phenotype association analysis provide the tools necessary to estimate h^2, and to identify large-effect loci (and to estimate their allele frequencies) where they exist (Yang *et al.* 2014; Funk *et al.* 2018).

Why do polygenic architectures usually confer increased population viability compared to genetic architectures including large-effect loci? This pattern arises in part from a slower and less variable decline in h^2 during adaptation for polygenic traits than for traits with large-effect loci (Figures S3, S5, S6, S7). The rapid decline in h^2 when large-effect beneficial alleles are already common, and the frequent loss of initially rare large-effect alleles means that there is a narrow window of p_0 where traits with large-effect architectures are likely to evolve in response to selection as fast or faster than polygenic traits. Holding the initial heritability constant, the potential scope for adaptive phenotypic change is considerably smaller when large-effect loci are present compared to a polygenic architecture (Figures S1). Additionally, evolutionary and demographic responses to selection appear to be more stochastic in populations with large-effect loci (Figure 3). This suggests that reliably predicting population responses to selection will be more difficult when large-effect loci are present, particularly when the initial frequency of large effect alleles is not known precisely. These results highlight the importance of identifying large-effect loci where they exist, and using information on their effect-sizes and allele frequencies along with h_0^2 in models predicting demographic responses to environmental change. Predictions

of population responses to selection that do not account for the strong effects of genetic architecture on the temporal dynamics of h^2 and adaptation are likely to be misleading.

Understanding how populations will respond to environmental change is both challenging and vitally important in conservation and evolutionary ecology (Urban *et al.* 2016). Reliable predictions of how biodiversity will respond to large-scale environmental change are necessary to efficiently prioritize scarce conservation resources and to develop effective strategies to conserve populations, and to mitigate inevitable biodiversity losses. However, there are considerable obstacles to reliably predicting responses to selection. For example, the complex and interacting effects of environmental stochasticity, genotype-by-environment interactions, phenotypic plasticity, pleiotropy, dominance interactions, gene flow, simultaneous selection on multiple potentially correlated traits, and changing community structure (i.e., species interactions) can all strongly affect adaptation and population dynamics, but are also difficult to measure and to forecast into the future. Reliable predictions of biological responses to environmental change in the wild will therefore be difficult to achieve, even in well-studied systems where the heritability, genetic architecture, and fitness effects of the relevant phenotype(s) are known. It will often be difficult or impossible to reliably predict how wild populations will respond to large-scale environmental change. We therefore encourage caution when attempting to predict eco-evolutionary dynamics under climate change and other human-driven environmental changes.

Our results uncover a likely widespread phenomenon where, for a given h^2 starting condition, polygenic architectures can often confer substantially higher population viability under rapidly shifting phenotypic optima compared to genetic architectures with large-effect loci. Incorporating these effects of genetic architecture into population viability models (e.g., using the modelling approaches presented here) could substantially advance understanding of the consequences of human-driven environmental change for species survival and biodiversity conservation. Improved understanding of vulnerability to environmental change could also advance strategies to conserve vital natural and agricultural resources (Aitken & Whitlock 2013; Flanagan *et al.* 2017; Funk *et al.* 2018), for example by identifying populations and species to prioritize for conservation action.

ACKNOWLEDGEMENTS
M.K. was supported by Montana Fish, Wildlife & Parks. G.L. and M.K. were supported partially by National Science Foundation grant DoB-1639014, and National Aeronautics and Space Administration grant NNX14AB84G. We thank Fred W. Allendorf, Matthew Jones, L. Scott Mills, Alden Wright, Jeff Hard, and Robin Waples for helpful discussions and/or comments on a previous version of the manuscript.

DATA AVAILABILITY: This manuscript is based on mathematical models and simulations and does not include any empirical data. R packages implementing the models are freely available at https://github.com/martykardos/geneticArchPopDynamics, and will be placed in a permanent archive upon acceptance.

AUTHOR CONTRIBUTIONS: M.K. conceived the study. M.K. and G.L. designed the study. M.K. wrote and analyzed the mathematical models and simulations. M.K. and G.L. wrote the paper.

REFERENCES

Aitken, S.N. & Whitlock, M.C. (2013). Assisted gene flow to facilitate local adaptation to climate change. *Annual Review of Ecology, Evolution, and Systematics*, 44, 367-388

Alberto, F.J., Aitken, S.N., Alía, R., González-Martínez, S.C., Hänninen, H., Kremer, A. *et al.* (2013). Potential for evolutionary responses to climate change–evidence from tree populations. *Global Change Biology*, 19, 1645-1661.

Barson, N.J., Aykanat, T., Hindar, K., Baranski, M., Bolstad, G.H., Fiske, P. *et al.* (2015). Sex-dependent dominance at a single locus maintains variation in age at maturity in salmon. *Nature*, 528, 405-408.

Barton, N. & Turelli, M. (1991). Natural and sexual selection on many loci. *Genetics*, 127, 229-255.

Barton, N.H. & Keightley, P.D. (2002). Multifactorial genetics: understanding quantitative genetic variation. *Nature Reviews Genetics*, 3, 11-21.

Bay, R.A., Rose, N.H., Logan, C.A. & Palumbi, S.R. (2017). Genomic models predict successful coral adaptation if future ocean warming rates are reduced. *Science Advances*, 3, e1701413.

Boyle, E.A., Li, Y.I. & Pritchard, J.K. (2017). An expanded view of complex traits: from polygenic to omnigenic. *Cell*, 169, 1177-1186.

Bürger, R. & Lynch, M. (1995). Evolution and extinction in a changing environment: a quantitative-genetic analysis. *Evolution*, 49, 151-163.

Chevin, L.-M., Lande, R. & Mace, G.M. (2010). Adaptation, plasticity, and extinction in a changing environment: towards a predictive theory. *PLoS Biology*, 8, e1000357.

Chevin, L.M. & Lande, R. (2010). When do adaptive plasticity and genetic evolution prevent extinction of a density-regulated population? *Evolution*, 64, 1143-1150.

Efron, B. & Tibshirani, R.J. (1994). *An introduction to the bootstrap*. Chapman & Hall/CRC, Boca Raton, Florida.

Epstein, B., Jones, M., Hamede, R., Hendricks, S., McCallum, H., Murchison, E.P. *et al.* (2016). Rapid evolutionary response to a transmissible cancer in Tasmanian devils. *Nature Communications*, 7, 12684.

Fadlallah, Y.H. (1983). Population dynamics and life history of a solitary coral, *Balanophyllia elegans*, from Central California. *Oecologia*, 58, 200-207.

Falconer, D.S. & Mackay, T.F.C. (1996). *Introduction to quantitative genetics*. 4 edn. Pearson.

Flanagan, S.P., Forester, B.R., Latch, E.K., Aitken, S.N. & Hoban, S. (2017). Guidelines for planning genomic assessment and monitoring of locally adaptive variation to inform species conservation. *Evolutionary Applications*, 11, 1035–1052.

Funk, W., Forester, B.R., Converse, S.J., Darst, C. & Morey, S. (2018). Improving conservation policy with genomics: a guide to integrating adaptive potential into US Endangered Species Act decisions for conservation practitioners and geneticists. *Conservation Genetics*, 20, 115-134.

Gomulkiewicz, R. & Holt, R.D. (1995). When does evolution by natural selection prevent extinction? *Evolution*, 49, 201-207.

Gomulkiewicz, R., Holt, R.D., Barfield, M. & Nuismer, S.L. (2010). Genetics, adaptation, and invasion in harsh environments. *Evolutionary Applications*, 3, 97-108.

Hansen, T.F., Pélabon, C. & Houle, D. (2011). Heritability is not evolvability. *Evolutionary Biology*, 38, 258-277.

Johnston, S.E., Gratten, J., Berenos, C., Pilkington, J.G., Clutton-Brock, T.H., Pemberton, J.M. *et al.* (2013). Life history trade-offs at a single locus maintain sexually selected genetic variation. *Nature*, 502, 93-95.

Jones, M.R., Mills, L.S., Alves, P.C., Callahan, C.M., Alves, J.M., Lafferty, D.J. *et al.* (2018). Adaptive introgression underlies polymorphic seasonal camouflage in snowshoe hares. *Science*, 360, 1355-1358.

Kardos, M., Luikart, G., Bunch, R., Dewey, S., Edwards, W., McWilliam, S. *et al.* (2015). Whole-genome resequencing uncovers molecular signatures of natural and sexual selection in wild bighorn sheep. *Molecular Ecology*, 24, 5616-5632.

Kimura, M. (1984). *The neutral theory of molecular evolution*. Cambridge University Press.

Lamichhaney, S., Berglund, J., Almén, M.S., Maqbool, K., Grabherr, M., Martinez-Barrio, A. *et al.* (2015). Evolution of Darwin's finches and their beaks revealed by genome sequencing. *Nature*, 518, 371-375.

Lamichhaney, S., Fan, G., Widemo, F., Gunnarsson, U., Thalmann, D.S., Hoeppner, M.P. *et al.* (2016). Structural genomic changes underlie alternative reproductive strategies in the ruff (*Philomachus pugnax*). *Nature Genetics*, 48, 84-88.

Lande, R. (1983). The response to selection on major and minor mutations affecting a metrical trait. *Heredity*, 50, 47-65.

Llaurens, V., Whibley, A. & Joron, M. (2017). Genetic architecture and balancing selection: the life and death of differentiated variants. *Molecular Ecology*, 26, 2430-2448.

Lynch, M., Gabriel, W. & Wood, A.M. (1991). Adaptive and demographic responses of plankton populations to environmental change. *Limnology and Oceanography*, 36, 1301-1312.

Lynch, M. & Lande, R. (1993). Evolution and extinction in response to environmental change. In: *Biotic interactions and global change.* United States, pp. 234-250.

May, R.M. (1974). Biological populations with nonoverlapping generations: stable points, stable cycles, and chaos. *Science*, 186, 645-647.

Mduma, S.A., Sinclair, A. & Hilborn, R. (1999). Food regulates the Serengeti wildebeest: a 40-year record. *Journal of Animal Ecology*, 68, 1101-1122.

Mills, L.S., Bragina, E.V., Kumar, A.V., Zimova, M., Lafferty, D.J., Feltner, J. *et al.* (2018). Winter color polymorphisms identify global hot spots for evolutionary rescue from climate change. *Science*, 359, 1033-1036.

Nadeau, C.P. & Urban, M.C. (2019). Eco-evolution on the edge during climate change. *Ecography*, 42, 1-18.

Nunney, L. (2015). Adapting to a changing environment: modeling the interaction of directional selection and plasticity. *Journal of Heredity*, 107, 15-24.

Pease, C.M., Lande, R. & Bull, J.J. (1989). A model of population growth, dispersal and evolution in a changing environment. *Ecology*, 70, 1657-1664.

Shaw, R.G. (2019). From the past to the future: considering the value and limits of evolutionary prediction. *The American Naturalist*, 193, 1-10.

Stockwell, C.A., Hendry, A.P. & Kinnison, M.T. (2003). Contemporary evolution meets conservation biology. *Trends in Ecology & Evolution*, 18, 94-101.

Thompson, T.Q., Bellinger, M.R., O'Rourke, S.M., Prince, D.J., Stevenson, A.E., Rodrigues, A.T. *et al.* (2019). Anthropogenic habitat alteration leads to rapid loss of adaptive variation and restoration potential in wild salmon populations. *Proceedings of the National Academy of Sciences*, 116, 177-186.

Urban, M.C., Bocedi, G., Hendry, A.P., Mihoub, J.-B., Pe'er, G., Singer, A. *et al.* (2016). Improving the forecast for biodiversity under climate change. *Science*, 353, aad8466.

Walsh, B. & Lynch, M. (2018). *Evolution and selection of quantitative traits*. Oxford University Press.

Yang, J., Zaitlen, N.A., Goddard, M.E., Visscher, P.M. & Price, A.L. (2014). Advantages and pitfalls in the application of mixed-model association methods. *Nature Genetics*, 46, 100-106.

FIGURES

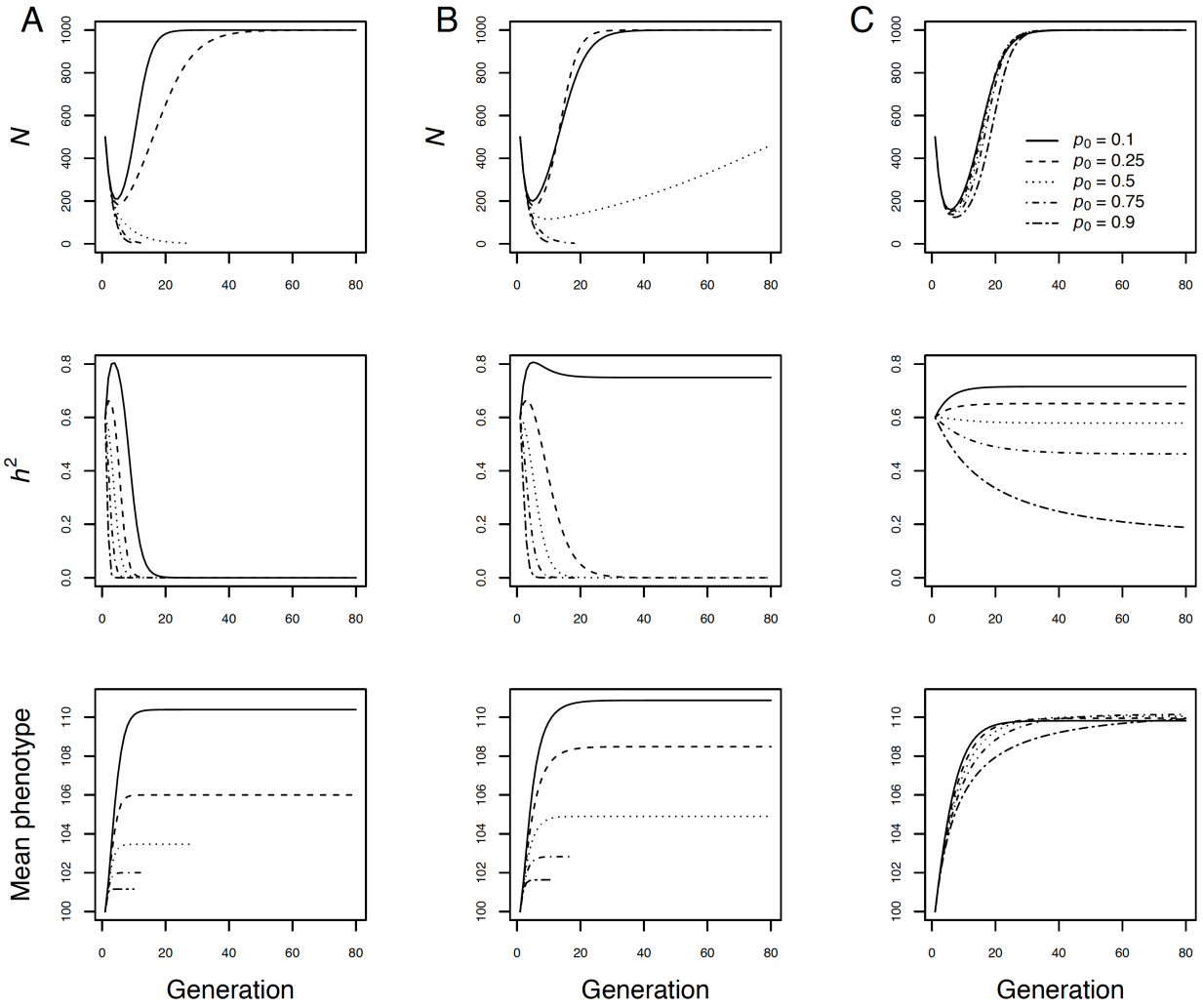

Figure 1. Numerical predictions of temporal changes in population size (N, top row), trait heritability (h^2, middle row), and mean phenotype (bottom row) in density-regulated populations with a single large-effect locus (**A**), two large-effect loci (**B**), and 100 small-effect loci (**C**) affecting a quantitative trait under selection after a sudden environmental change. Initial population size was $N = 500$ with carrying capacity of $K = 1{,}000$, and the initial heritability was $h_0^2 = 0.6$ in all cases. The optimum phenotype shifted from $\theta_0 = 100$ to $\theta_1 = 110$ in the first generation. Line types indicate the initial frequencies of the positively selected allele(s) conferring a larger phenotype, as indicated in the legend.

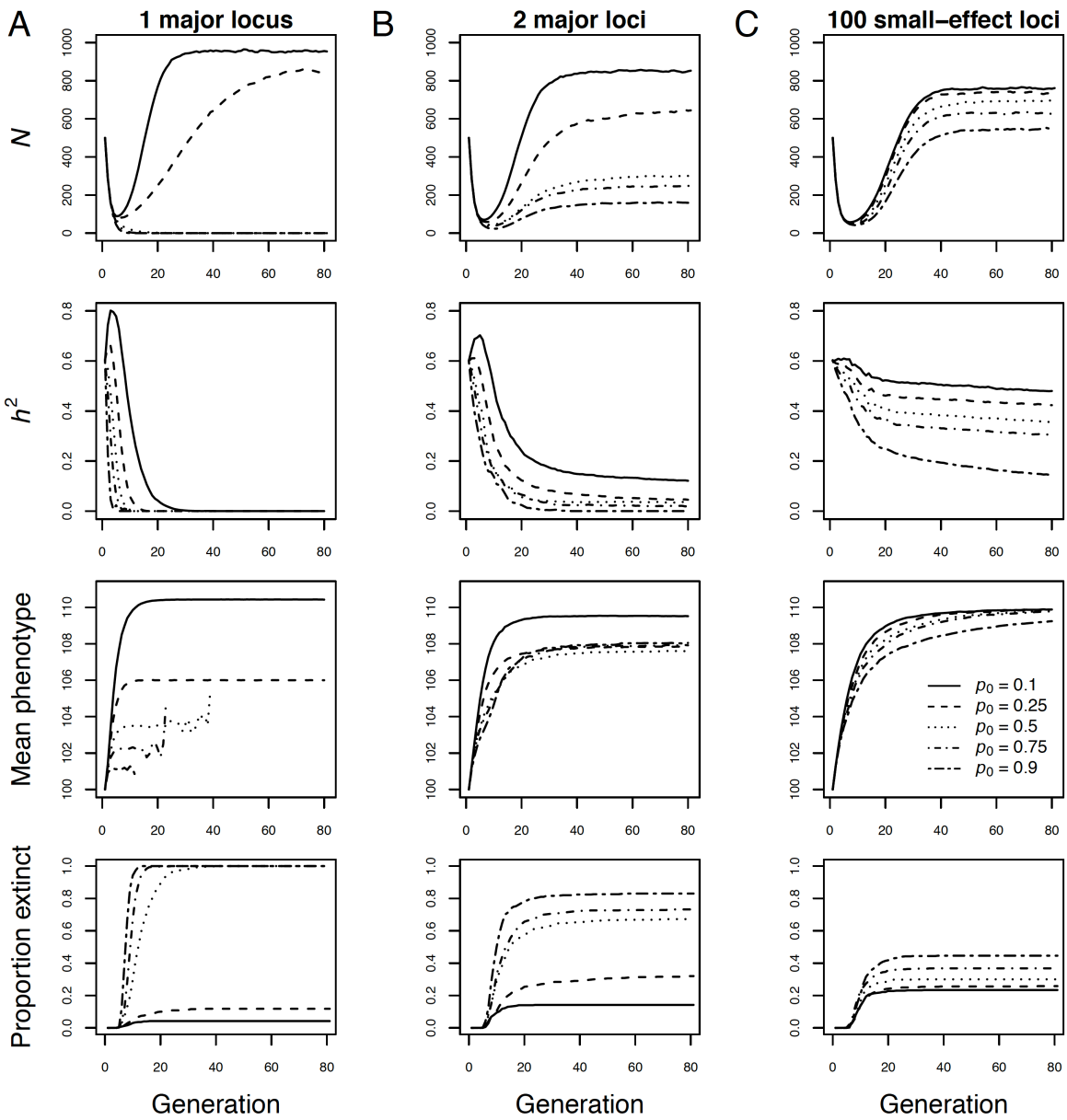

Figure 2. Individual-based simulations of evolutionary and population dynamics in density-regulated populations with a single large-effect locus (**A**), two large-effect loci (**B**), and 100 small-effect loci (**C**) affecting a quantitative trait under selection after a sudden environmental change. The optimum phenotype shifted from $\theta_0 = 100$ to $\theta_1 = 110$ in the first generation. Initial population size was $N_0 = 500$, and capacity was $K = 1{,}000$. The initial heritability was $h_0^2 = 0.6$ in all cases. Line types indicate the initial frequency of the positively selected allele(s) conferring a larger phenotype as indicated in the legend.

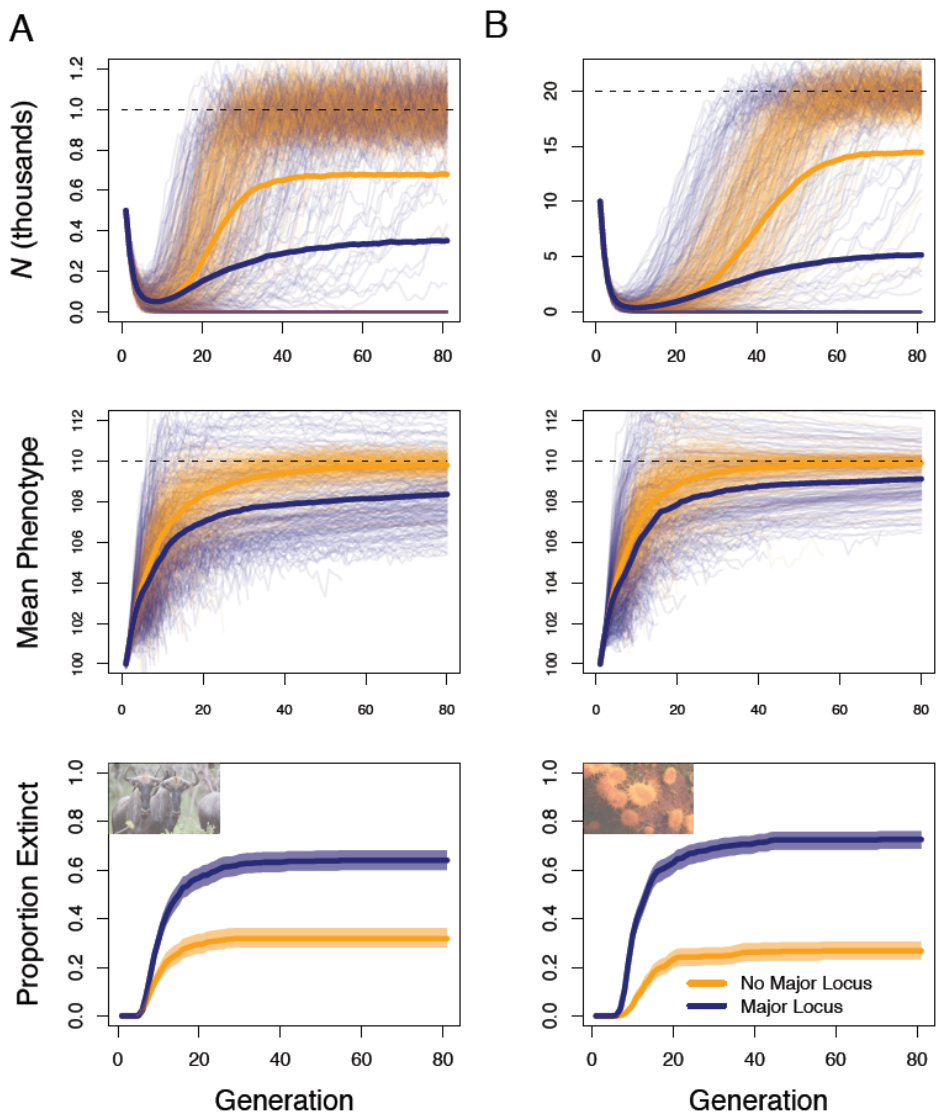

Figure 3. Effects of genetic architecture on phenotypic evolution and population dynamics in closed populations with life histories approximating large mammals (**A**), and corals (**B**). Results are shown in blue for populations with a large-effect locus, and in orange for populations where the selected trait was polygenic. The phenotypic optimum permanently shifted from its initial value $\theta_0 = 100$ to $\theta_1 = 110$ in generation one. The initial heritability was $h_0^2 = 0.6$. Thin lines show the population size (top row) and mean phenotype (middle row) through time. Thick lines show the mean population size and phenotype across all 500 repetitions. The bottom panels show the proportion of extinct populations through time, with percentile bootstrap 95% confidence intervals.

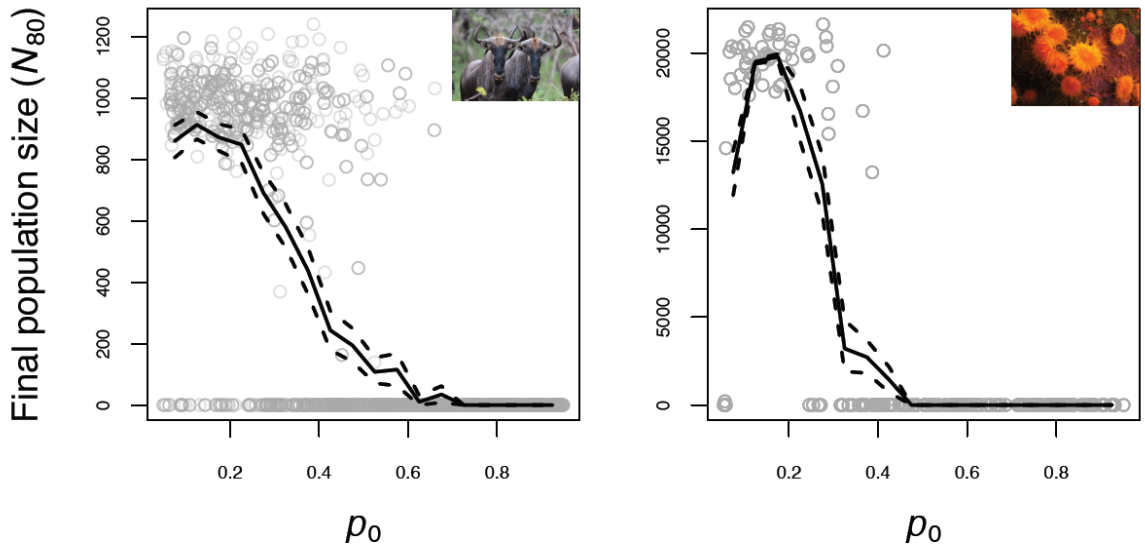

Figure 4. Effects of the initial large-effect allele frequency (p_0) on final population size in simulations with approximate large mammal (**A**) and coral (**B**) life histories. The y-axis represents the final population size at generation 80 (N_{80}), and the x-axis shows the large-effect allele p_0. The solid lines represent the mean N_{80} across 2,000 simulation repetitions in non-overlapping p_0 windows of width 0.05. Dashed lines are 95% percentile bootstrap confidence intervals for mean N_{80}.

SUPPLEMENTARY MATERIALS

The genetic architecture of fitness drives population viability during rapid environmental change

Marty Kardos[1*], Gordon Luikart[1]

[1]University of Montana, Division of Biological Sciences, Flathead Lake Biological Station, 32125 Biostation Lane, Polson, MT 59860, USA
*Correspondence: marty.kardos@mso.umt.edu

Effects of gene flow on the influence of genetic architecture on population viability
Previous work suggests that selection with gene flow can favor the evolution of genetic architectures with large-effect loci (Yeaman & Whitlock, 2011). The presence of large-effect loci may therefore confer more robust evolutionary and demographic responses to selection when there is gene flow from populations with a different phenotypic optimum. We ran simulations equivalent to our individual-based simulations with a large mammal-like life history in the main text, except with immigration (either 4 or 8 immigrants/generation) from a population where the phenotypic optimum remained at $\theta = 100$ instead of shifting to $\theta_1 = 110$ in the first generation.

The polygenic trait architecture conferred higher population viability in populations with immigration from a population with a different phenotypic optimum. However, this effect was weaker compared to our results from populations without immigration. The extinction rate was 55% among populations with a polygenic architecture, and 76% in populations with a large-effect locus when the immigration rate was four individuals per generation (Figure S9). With a higher immigration rate of 8 individuals per generation, the extinction rate was 48% among populations with the polygenic architecture, and 74% in populations with a large-effect locus (Figure S10). These results are likely due to immigration more effectively countering adaptative allele frequency changes at individual loci with small effects compared to large-effect loci (Yeaman & Whitlock, 2011).

Effects of major locus effect size on population viability
We then evaluated the influence of the major locus effect sizes on evolutionary and demographic responses to selection. We ran our simulations of large mammals with the large-effect locus responsible for 50%, 70% and 90% of h_0^2 and compared the results to simulations where the selected trait was polygenic. In all cases, the response to selection was stronger for the polygenic architecture than when there was a large-effect locus. The extinction rates were 1.28, 1.84, and 2.01 times higher with large-effect loci responsible for 50%, 70%, and 90% of h_0^2, respectively, compared to the polygenic architecture (extinction rate = 0.32, Figure S11).

Effects of genetic architecture on population viability with a temporally increasing and stochastic phenotypic optimum value
Our analyses in the main text of the paper focused on the simple scenario where selection is induced by a sudden and permanent environmental change. However, environmental change is

often stochastic and spread out over long periods of time. We therefore used our individual-based simulation model with a large mammal-like life history to evaluate the effects of genetic architecture on population dynamics under this type of environmental change. We ran simulations equivalent to those shown in Figure 3A in the main text, except here the phenotypic optimum increased linearly with time (from 100 to 110) over the first *x* generations, with an error term to incorporate temporal stochasticity. The phenotypic optimum value for generation *t* was calculated as

$$\theta_t = \begin{cases} \theta_0 + \frac{t}{x}(\theta_1 - \theta_0) + \varepsilon & \text{if } t < x \\ \theta_1 + \varepsilon & \text{if } t \geq x \end{cases} \qquad \text{(S1)}$$

where θ_0 is the initial phenotypic optimum, θ_1 is the final deterministic phenotypic optimum value, and ε is normally distributed with mean of zero and standard deviation of 2. We ran 500 simulation replicates with $x = 10$ generations, and also with $x = 20$ generations. The results are show below in Figure S12, and were qualitatively equivalent to those presented in Figure 3A in the main text.

Effects of genetic architecture on population viability with linked loci

Our analyses in the main text assumed that loci were unlinked. Linkage disequilibrium arising from having linked fitness-related loci can affect the response to selection (Betancourt & Presgraves, 2002). We therefore ran simulations equivalent to those shown in Figure 3A, except here we placed the selected loci randomly across 10 chromosomes, each with a genetic length of 50 cM and physical length of 100 Mb, randomly selected crossover locations, and a Poisson distributed number of crossovers per meiosis. The results are shown in Figure S13 below, and were nearly identical to those in Figure 3A.

Effects of the genetic architecture on population viability with phenotypic plasticity

A previous theoretical population genetic model suggested that loci with large effects may provide higher adaptive potential and population viability when the selected phenotype is plastic (Nunney, 2015). We therefore tested effects of genetic architecture in the presence of phenotypic plasticity. We used a model of plasticity similar to that of Nunney (Nunney, 2015). Specifically, we modified equation (10) from the main text to incorporate a linear effect of the optimal phenotype on the realized phenotype as

$$z_i = \theta_0 - \bar{G}_0 + \sum_{j=1}^{n} c_{ji}\, a_j + m\left(\theta_t - \left[\theta_0 - \bar{G}_0 + \sum_{j=1}^{n} c_{ji}\, a_j\right]\right) + \varepsilon_i, \qquad \text{(S2)}$$

where *m* is the rate of change in expected phenotype per unit difference between the optimal phenotype and individual *i*'s expected phenotype in the absence of plasticity. The plasticity model is shown with examples in Figure S15 below. We ran 500 simulation replicates equivalent to those described above (where there is a stochastic and linear increase in θ with time) except here we considered values of $m = 0.1$, 0.2, and 0.4. The results from these simulations are consistent with the results above and in the main text (e.g., Figure 3). The polygenic architecture on average conferred higher population sizes and a lower extinction rate than when there was a

large-effect locus in simulations with m = 0.1, and m = 0.2 (Figure S16). The extinction rate was <0.05 for both genetic architectures when phenotypic plasticity was strong (m = 0.4).

SUPPLEMENTARY FIGURES

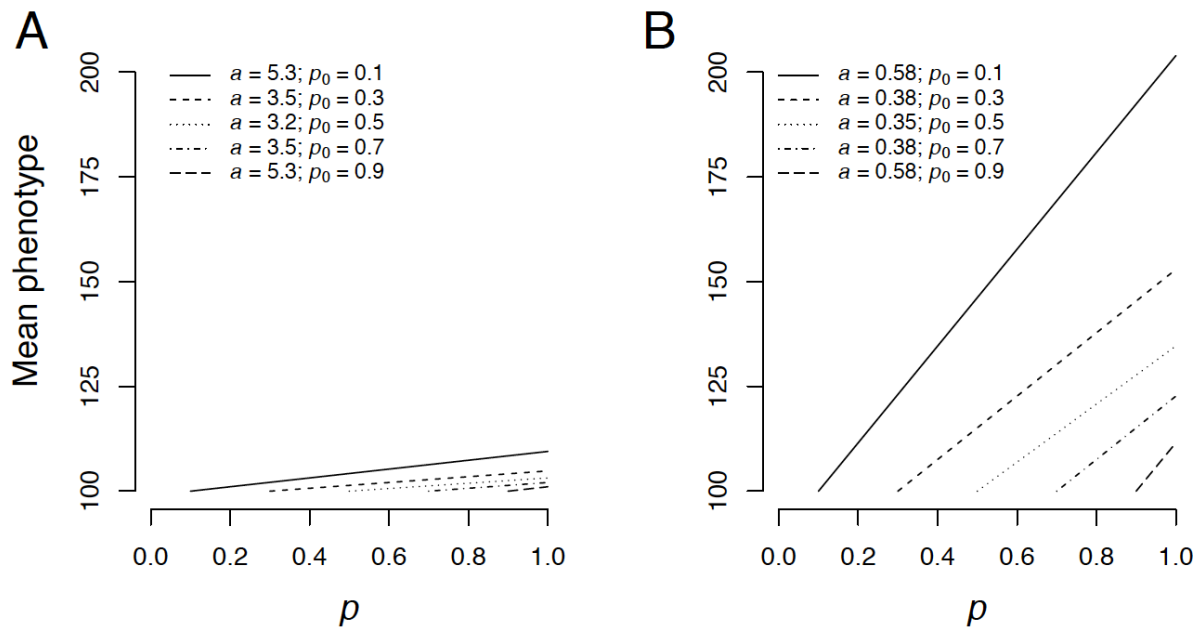

Figure S1. Evolutionary potential in populations with a single large-effect locus (**A**), and 100 small-effect loci (**B**) controlling a phenotypic trait under directional viability selection. The initial heritability was h_0^2 = 0.5, and the initial total phenotypic variance was V_P = 10 in all cases. The expectations for potential phenotypic change as the positively selected allele(s) conferring a larger phenotype go from the initial frequency p_0 to fixation are shown for p_0 ranging from 0.1 to 0.9. Note that $h_0^2 = \frac{n(2p_0(1-p_0)a^2)}{V_P}$, where a is half the difference between alternative homozygous genotypes at each of n loci affecting the selected trait. Mating is assumed to be random and genotypes are assumed to be in Hardy-Weinberg proportions.

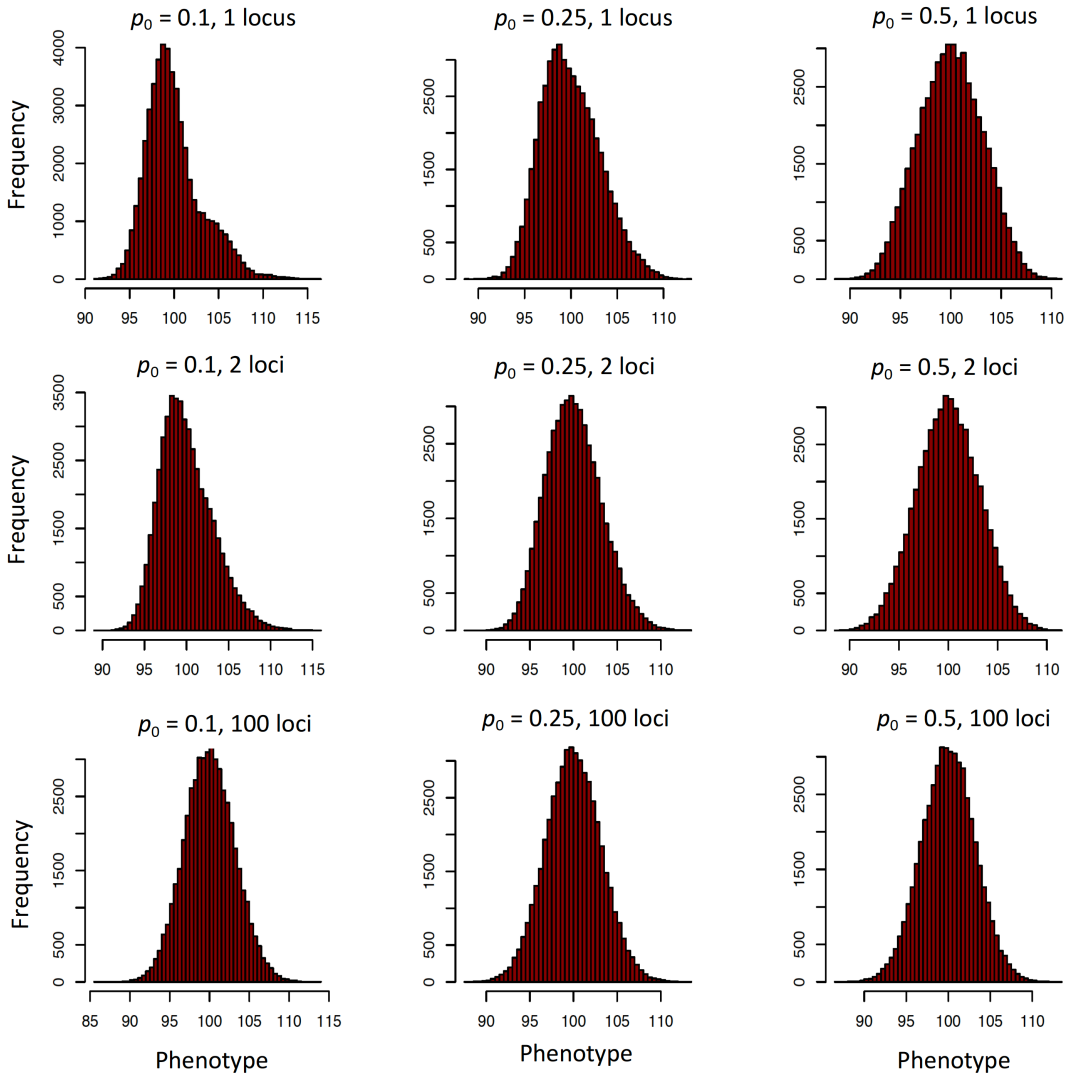

Figure S2. Distribution of simulated phenotypes. The simulated phenotype distributions are shown for three initial allele frequencies (p_0 = 0.1, 0.25, 0.5), and three numbers of loci contributing to the selected phenotype (n = 1, 2, and 100 loci). Each panel shows the distribution of 50,000 simulated phenotypes.

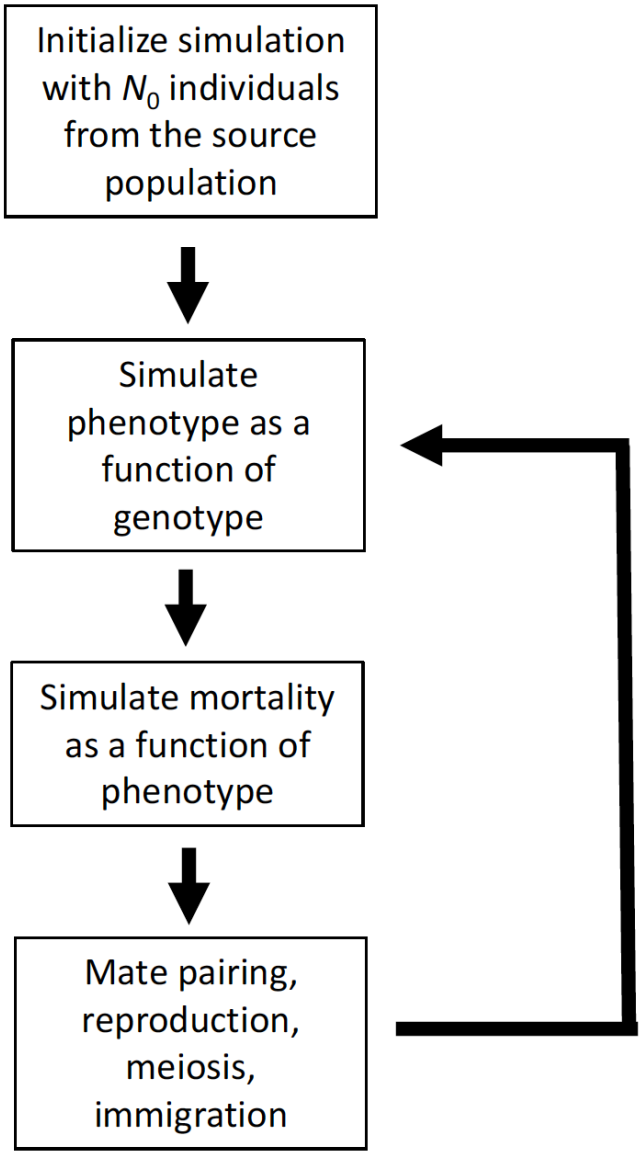

Figure S3. Flowchart of the sequence of events in the individual-based simulation model. Details of each step in the simulation procedure are described in detail in the Materials and Methods.

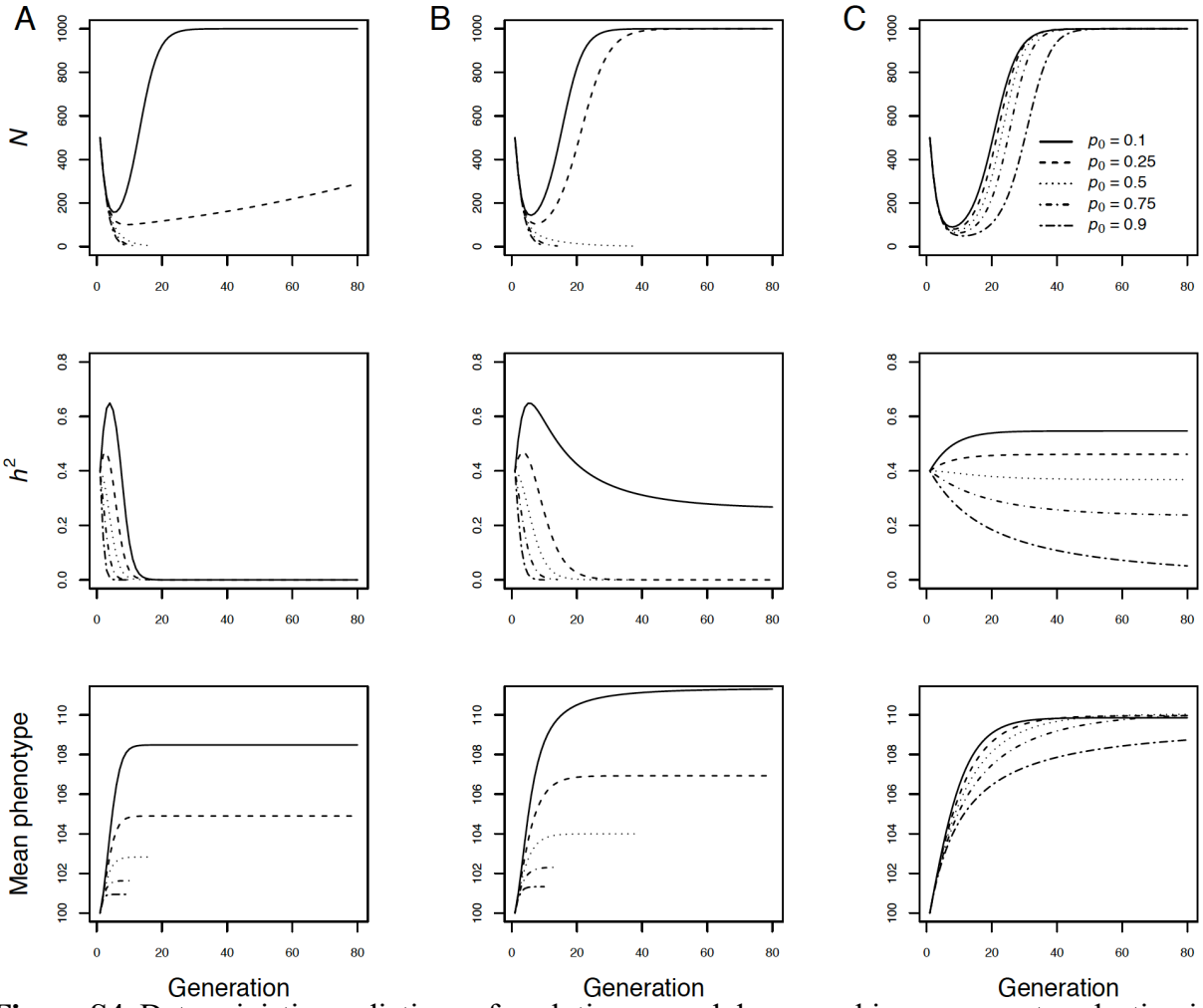

Figure S4. Deterministic predictions of evolutionary and demographic responses to selection in density-regulated populations with a single large-effect locus (**A**), two large-effect loci (**B**), and 100 small-effect loci (**C**) affecting a quantitative trait under directional selection after a sudden environmental change. The phenotypic optimum permanently shifted from its initial value $\theta_0 = 100$ to $\theta_1 = 110$ in generation one. The initial heritability was $h_0^2 = 0.4$ in all cases. Line types indicate the initial frequencies of the positively selected allele(s) conferring a larger phenotype as indicated in the legend. Initial population size was $N = 500$.

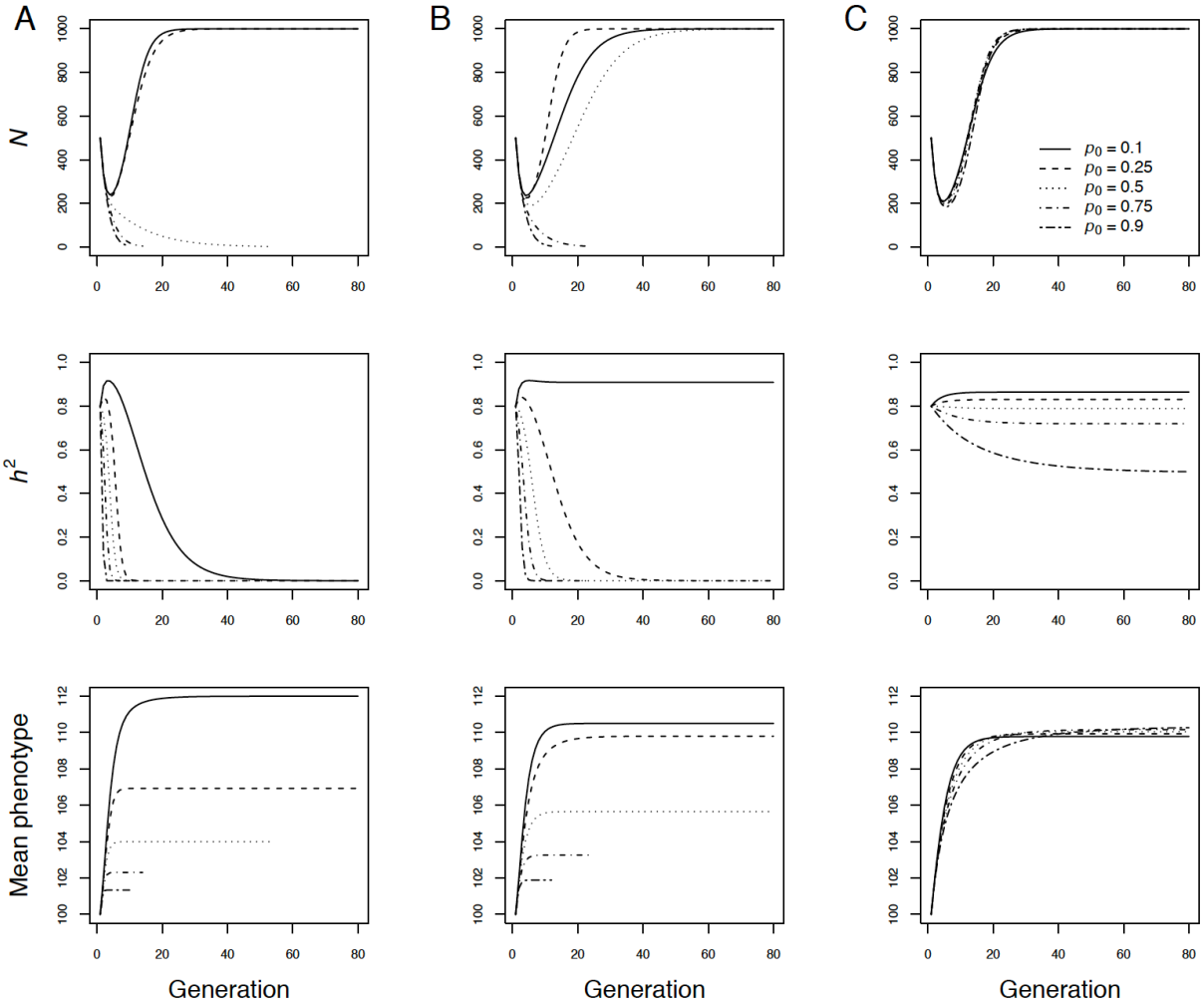

Figure S5. Deterministic predictions of evolutionary and demographic responses to selection in density-regulated populations with a single large-effect locus (**A**), two large-effect loci (**B**), and 100 small-effect loci (**C**) affecting a quantitative trait under directional selection after a sudden environmental change. The phenotypic optimum permanently shifted from its initial value $\theta_0 = 100$ to $\theta_1 = 110$ in generation one. The initial heritability was $h_0^2 = 0.8$ in all cases. Line types indicate the initial frequencies of the positively selected allele(s) conferring a larger phenotype as indicated in the legend. Initial population size was $N = 500$.

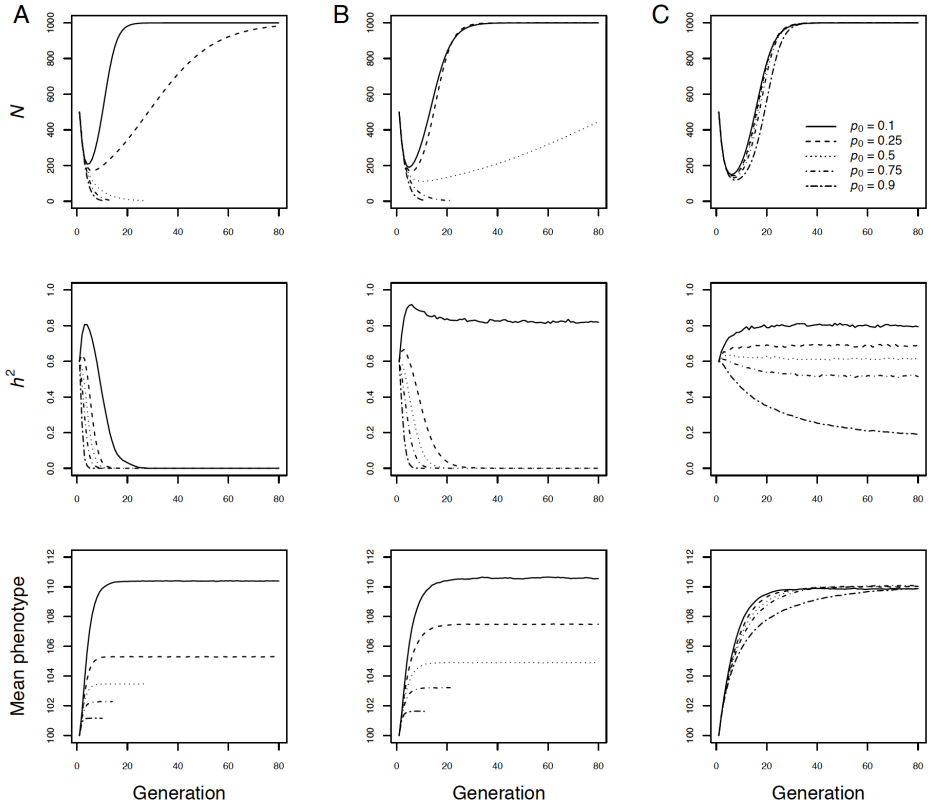

Figure S6. Evolutionary and demographic responses to a sudden change in the phenotypic optimum in density-regulated populations with a single large-effect locus (**A**), two large-effect loci (**B**), and 100 small-effect loci (**C**) affecting a quantitative trait under directional selection after a sudden environmental change. The lines in the first, second, and third rows show the mean population size, heritability, and mean phenotype across all 500 simulation repetitions versus time in generations. The initial heritability was h_0^2 = 0.6 in all cases. We varied the initial frequencies of the positively selected alleles conferring a larger phenotype from 0.1 to 0.9. Initial population size was N_0 = 500, and carrying capacity was K= 1,000. The phenotypic optimum permanently shifted from its initial value $\theta_0 = 100$ to $\theta_1 = 110$ in generation one. The model used here is identical to that used to produce the data shown in Figure 1 in the main text, except here we simulated the distributions of individual genotypes and phenotypes to account for any selection-induced linkage disequilibrium and deviations from the normality in the phenotypic distribution. Specifically, each generation we simulated the genotypes, phenotypes, and mating among 50,000 pseudo individuals. The genotypes in the first generation were initialized using the assumed p_0. The phenotypes were simulated following the individual-based quantitative genetic simulation model described in the main text. Offspring were assigned parents using weighted sampling (with the *sample* function in R), with the weights assigned based on phenotype using equation (1) in the main text. Population size in year t + 1 (N_{t+1}) was determined with equation (9) in the main text, with $\overline{w}_t$ replaced with the mean fitness among the 50,000 pseudo individuals in year t. This approach allowed us to precisely determine the expected distribution of individual fitness while accounting for any selection-induced linkage disequilibrium and non-normality in the phenotype distribution.

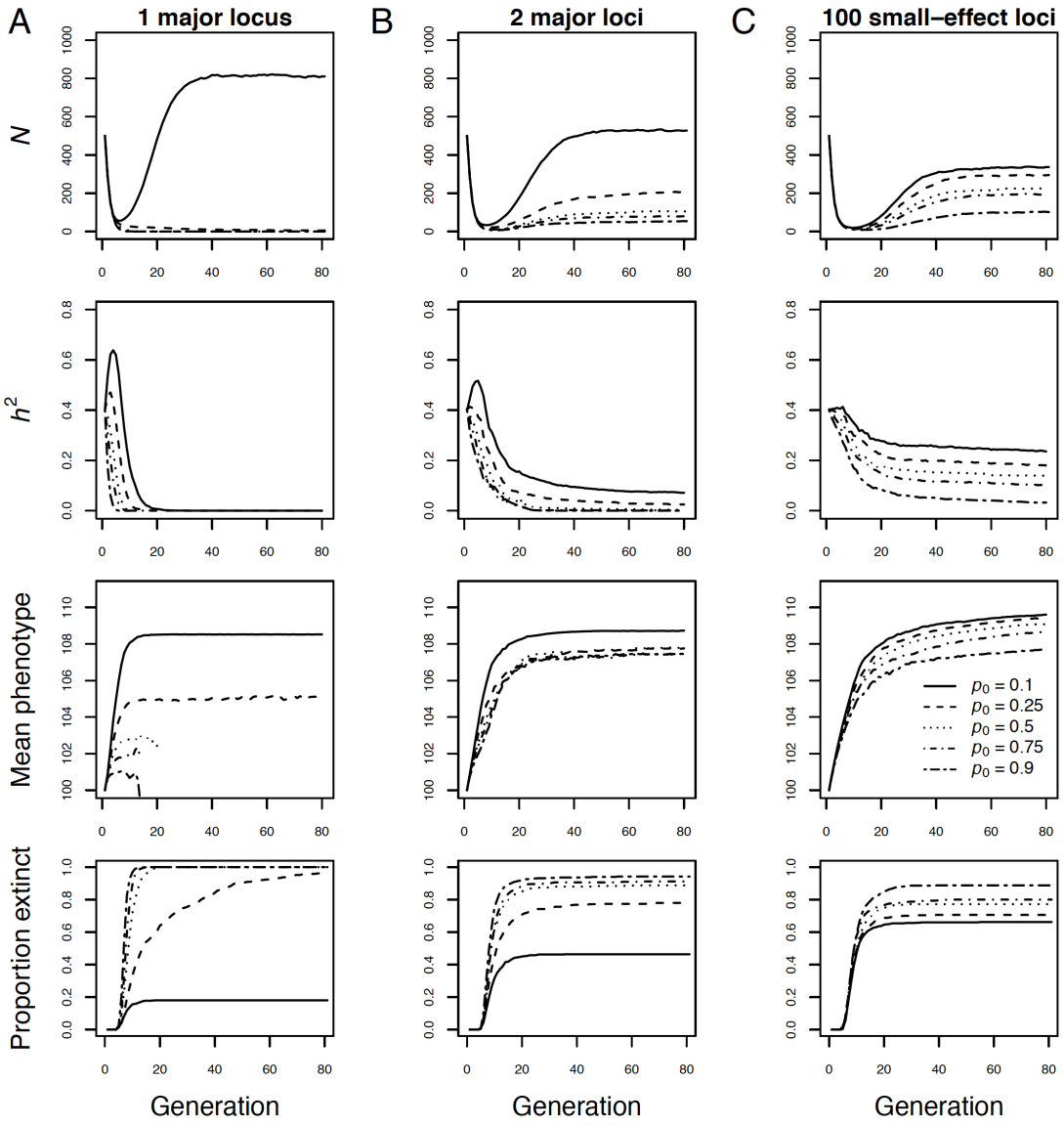

Figure S7. Individual-based simulations of evolutionary and demographic responses to directional selection in density-regulated populations with a single large-effect locus (**A**), two large-effect loci (**B**), and 100 small-effect loci (**C**) affecting a quantitative trait under directional selection after a sudden environmental change. The initial heritability was $h_0^2 = 0.4$ in all cases. The optimum phenotype shifted from its initial value $\theta_0 = 100$ to $\theta_1 = 110$ in the first generation. Line types indicate the initial frequencies of the positively-selected allele(s) conferring a larger phenotype. Initial population size was $N_0 = 500$, and carrying capacity was $K = 1{,}000$. The lines in the first, second, third, and fourth rows show the mean population size, heritability, mean phenotype, and proportion of extinction populations across all 500 simulation repetitions versus time in generations.

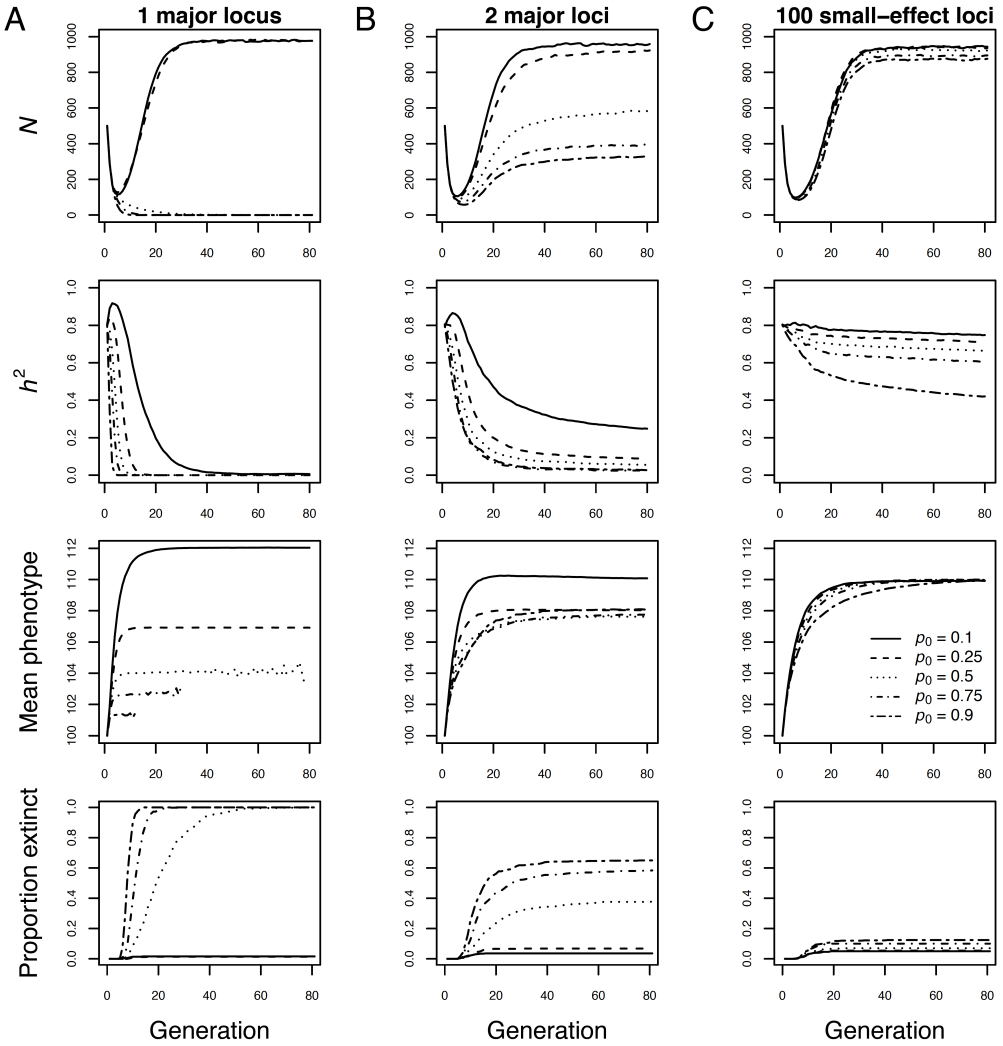

Figure S8. Individual-based simulations of evolutionary and demographic responses to directional selection in density-regulated populations with a single large-effect locus (**A**), two large-effect loci (**B**), and 100 small-effect loci (**C**) affecting a quantitative trait under directional selection after a sudden environmental change. The initial heritability was h_0^2 = 0.8 in all cases. The optimum phenotype shifted from its initial value $\theta_0 = 100$ to $\theta_1 = 110$ in the first generation. Line types indicate the initial frequencies of the positively selected allele(s) conferring a larger phenotype. Initial population size was N_0 = 500, and carrying capacity was K = 1,000. The lines in the first, second, third, and fourth rows show the mean population size, heritability, mean phenotype, and proportion of extinction populations across all 500 simulation repetitions versus time in generations.

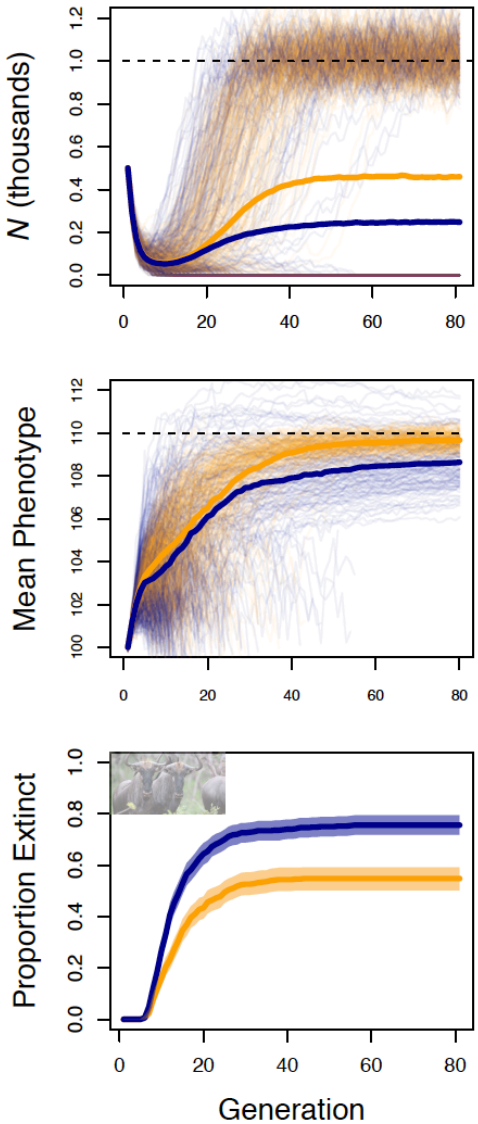

Figure S9. Effects of genetic architecture on phenotypic evolution and population dynamics in populations with an approximate large mammal life history and a low immigration rate (4 immigrants per generation) from a population with a constant phenotypic optimum of size $\theta = 100$. The optimum phenotype shifted from $\theta_0 = 100$ to $\theta_1 = 110$ in the focal population in the first generation. Results from populations with a large-effect locus are shown in blue; populations where the selected trait was polygenic are in orange. Thin lines show the population size (top row) and mean phenotype (middle row) through time. Thick lines show the mean population size and phenotype across all 500 repetitions. The bottom panels show the proportion of extinct populations through time, with bootstrap 95% confidence intervals.

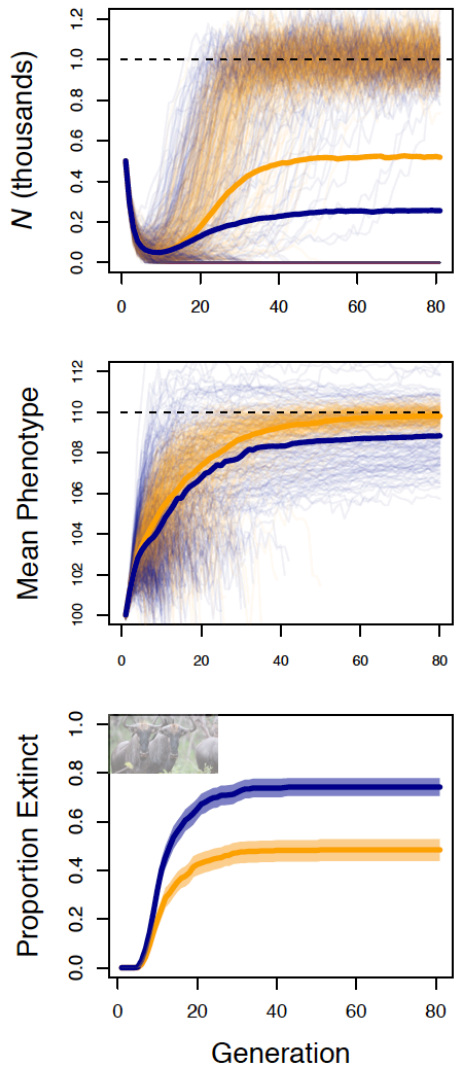

Figure S10. Effects of genetic architecture on phenotypic evolution and population dynamics in populations with an approximate large mammal life history and a high immigration rate (8 immigrants per generation) from a population with a constant phenotypic optimum of $\theta = 100$. The phenotypic optimum shifted from $\theta_0 = 100$ to $\theta_1 = 110$ in the focal population in the first generation of the simulations. Results from populations with a large-effect locus are shown in blue; populations where the selected trait was polygenic are in orange. Thin lines show the population size (top row) and mean phenotype (middle row) through time. Thick lines show the mean population size and phenotype across all 500 repetitions. The bottom panels show the proportion of extinct populations through time, with bootstrap 95% confidence intervals.

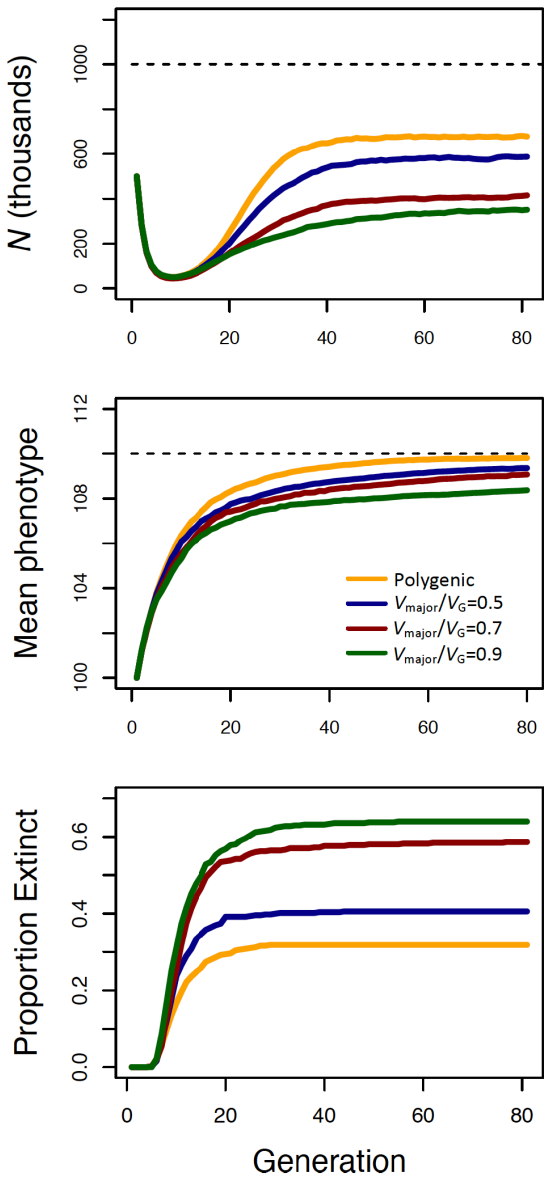

Figure S11. Influence of the effect size of large-effect loci on population dynamics.
The results are from simulations parameterized as in our simulations shown in Figure 3A, except here we varied the proportion of the genetic variance attributed to the large effect locus from $V_{\text{major}} = 0.5$ (blue), 0.7 (red), to 0.9 (green). The phenotypic optimum permanently shifted from its initial value $\theta_0 = 100$ to $\theta_1 = 110$ in generation one. Orange lines show results from simulations where there selected trait was polygenic (100 loci with equal and small effects). The bottom panel shows the proportion of extinct populations though time. These analyses are from 500 simulation repetitions for each of the four genetic architectures.

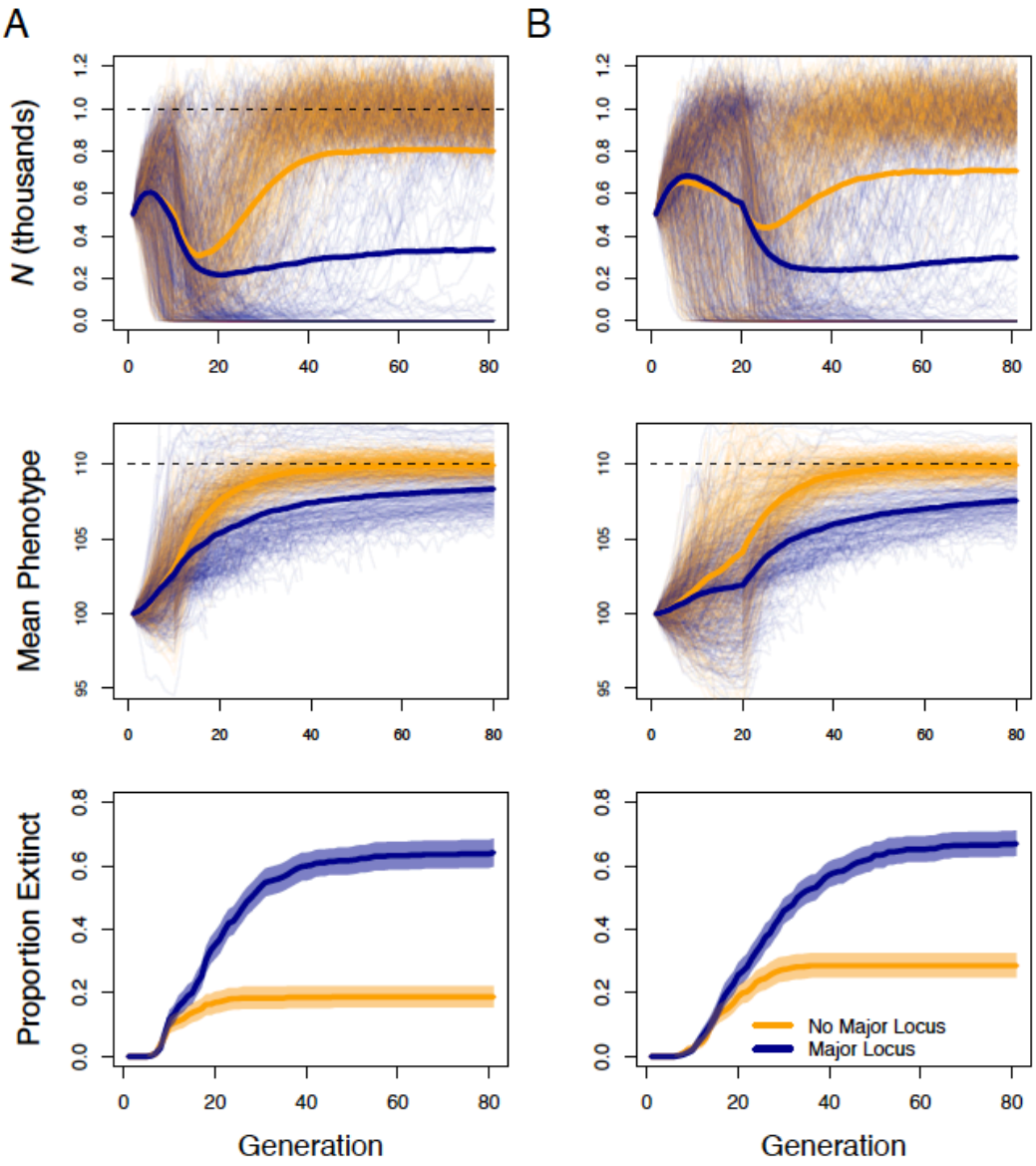

Figure S12. Effects of genetic architecture on phenotypic evolution and population dynamics in populations with a large mammal-like life history and with a stochastic linear increase in the optimum phenotype value with time. The optimum phenotype increased from $\theta_0 = 100$ to $\theta_1 = 110$ in the first either 10 (**A**) or 20 (**B**) generations. Results from populations with a large-effect locus are shown in blue; populations where the selected trait was polygenic are in orange. Thin lines show the population size (top row) and mean phenotype (middle row) through time. Thick lines show the mean population size and phenotype across all 500 repetitions. The bottom panels show the proportion of extinct populations through time, with bootstrap 95% confidence intervals.

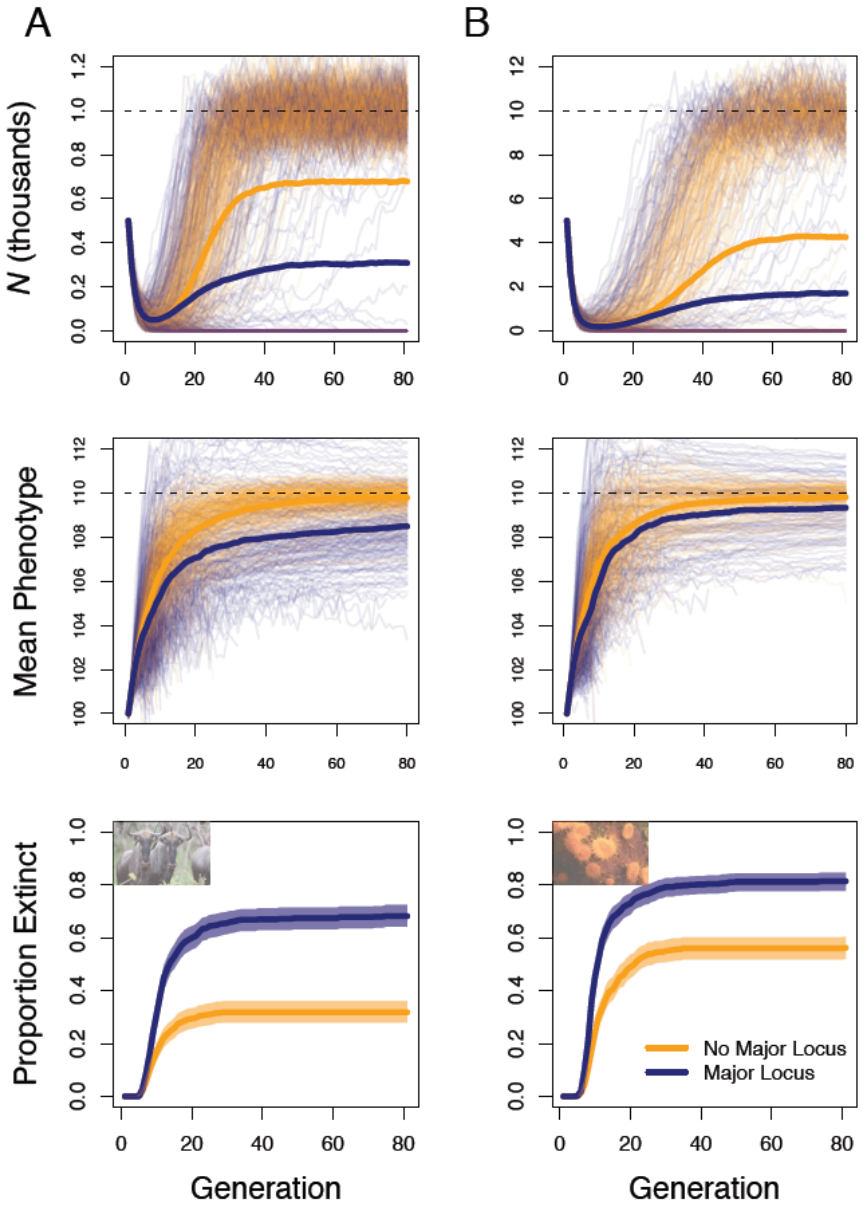

Figure S13 Effects of genetic architecture on phenotypic evolution and population dynamics with linked loci distributed over 10 chromosomes in closed populations with life histories approximating large mammals (**A**), and corals (**B**). The optimum phenotype shifted from $\theta_0 = 100$ to $\theta_1 = 110$ in the first generation. Results from populations with a large-effect locus are shown in blue; populations where the selected trait was polygenic are in orange. Thin lines show the population size (top row) and mean phenotype (middle row) through time. Thick lines show the mean population size across all simulation replicates. The bottom panels show the proportion of extinct populations through time, with bootstrap 95% confidence intervals.

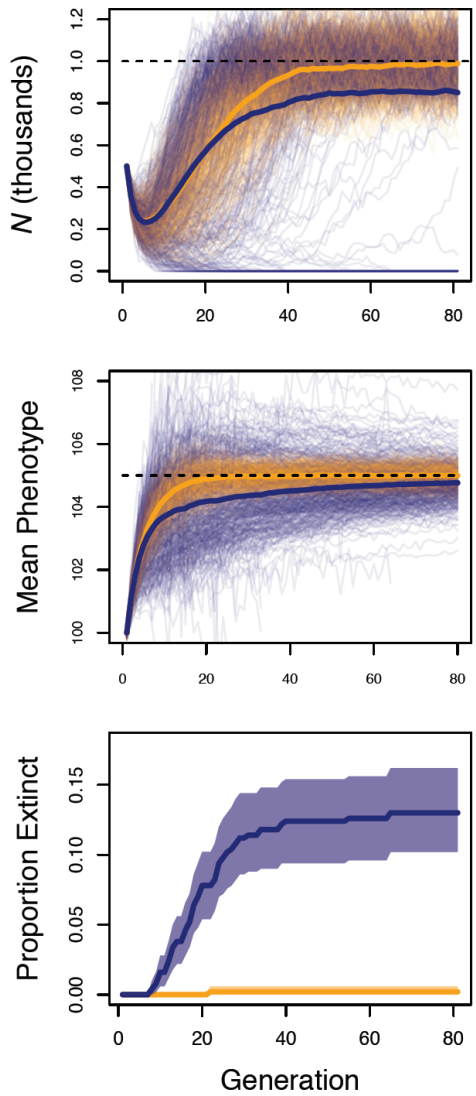

Figure S14. Effects of genetic architecture on phenotypic evolution and population dynamics in populations with a large mammal-like life history where the optimum phenotype shifted from $\theta_0 = 100$ to $\theta_1 = 105$ in the first generation (instead of $\theta_0 = 100$ to $\theta_1 = 110$ as in the previous simulations). Results from populations with a large-effect locus are shown in blue; populations where the selected trait was polygenic are in orange. Thin lines show the population size (top row) and mean phenotype (middle row) through time. Thick lines show the mean population size and phenotype across all 500 repetitions. The bottom panels show the proportion of extinct populations through time, with bootstrap 95% confidence intervals.

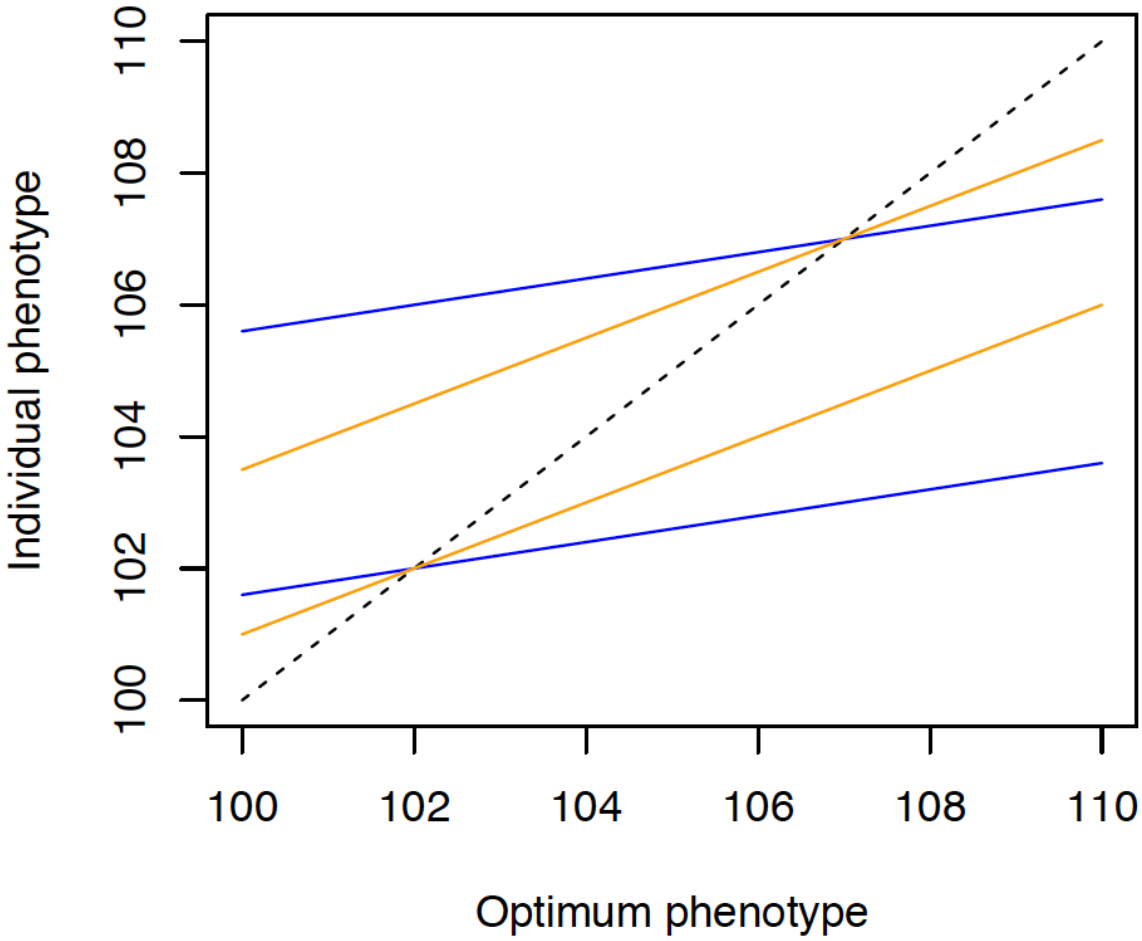

Figure S15. Model of plasticity shown as the individual phenotype plotted against the optimum phenotype. The dashed black line represents the case where individual phenotype equals the optimum phenotype. The expected phenotypes (i.e., ignoring random environmental effects) are shown for two individuals with breeding values of 102 and 107. The blue lines show the expected phenotypes with plasticity parameter $m = 0.2$, and the orange lines show the expected phenotypes with $m = 0.5$.

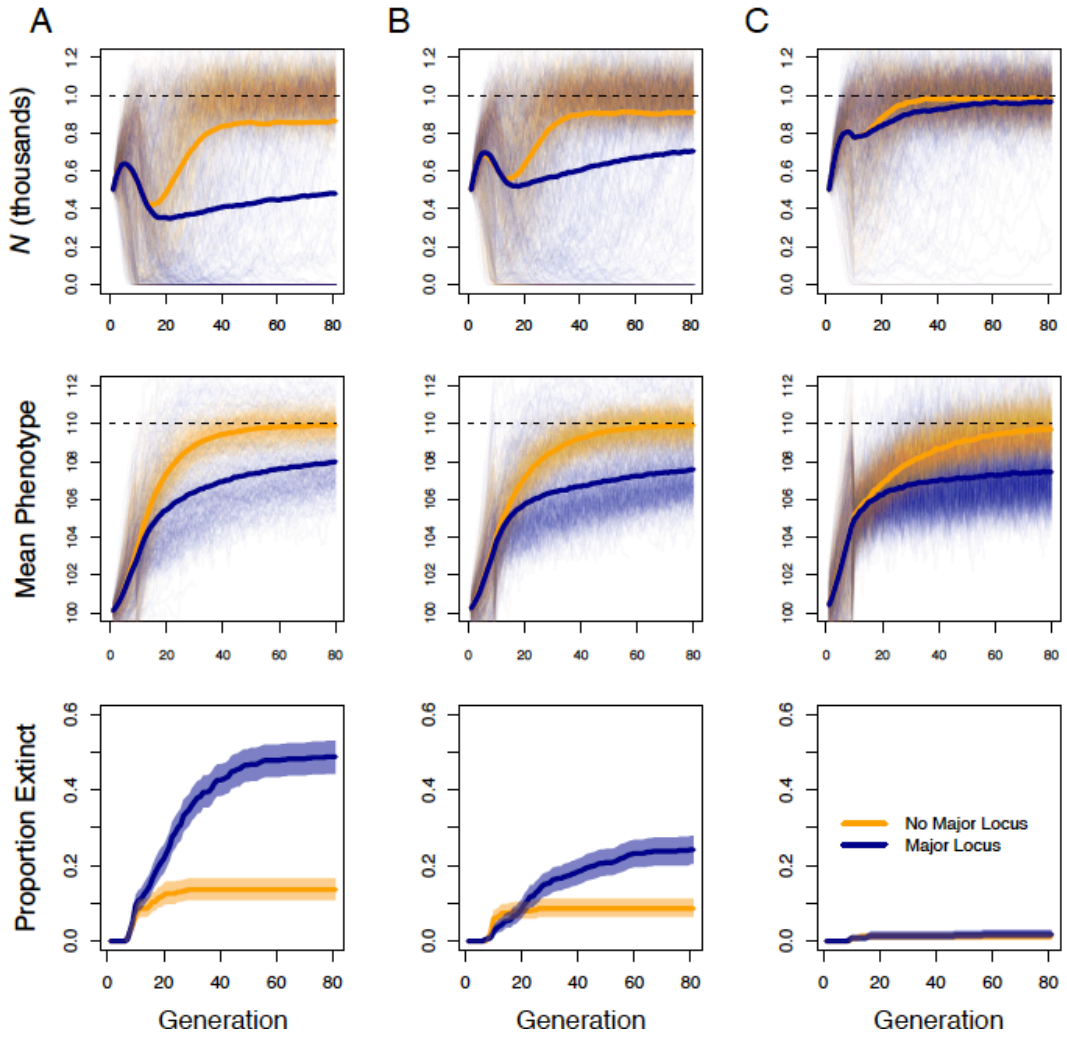

Figure S16. Effects of genetic architecture on phenotypic evolution and population dynamics in populations with life histories approximating large mammals and plasticity in the selected phenotype. Results are shown from simulations with the strength of plasticity set to $m = 0.1$ (**A**), $m = 0.2$ (**B**), $m = 0.4$ (**C**). There was a linear and stochastic increase in the optimum phenotype from $\theta_0 = 100$ to $\theta_1 = 110$ over the first 10 generations, as in Figure S12A above. Results from populations with a large-effect locus responsible for 90% of V_G are shown in blue; populations where the selected trait was polygenic are in orange. Thin lines show the population size (top row) and mean phenotype (middle row) through time for each simulation repetition. Thick lines show the mean population size and phenotype across all simulation replicates. The bottom panels show the proportion of extinct populations through time (thick lines), with the shaded areas representing 95% bootstrap confidence intervals.

References

Betancourt, A. J., & Presgraves, D. C. (2002). Linkage limits the power of natural selection in Drosophila. *Proceedings of the National Academy of Sciences, 99*(21), 13616-13620.

Nunney, L. (2015). Adapting to a changing environment: modeling the interaction of directional selection and plasticity. *Journal of Heredity, 107*(1), 15-24.

Yeaman, S., & Whitlock, M. C. (2011). The genetic architecture of adaptation under migration–selection balance. *Evolution: International Journal of Organic Evolution, 65*(7), 1897-1911.